An experimental and theoretical study of precipitation during tempering of martensite in Fe-C-Cr alloys

Ziyong Hou

Doctoral Thesis

Stockholm 2018

Unit of Structures

Department of Materials Science and Engineering

School of Industrial Engineering and Management

Royal Institute of Technology

SE-100 44 Stockholm

Sweden

Akademisk avhandling som med tillstånd av Kungliga Tekniska Högskolan i Stockholm, framläggs för offentlig granskning för avläggande av teknologie doktorsexamen fredagen den 14 September 2018, kl 10:00 i sal F3,Lindstedtsvägen 26, Kungliga Tekniska Högskolan, Stockholm

---

ISBN 978-91-7729-843-4

Ziyong Hou **An experimental and theoretical study of precipitation during tempering of martensite in Fe-C-Cr alloys**

Unit of Structures
Department of Materials Science and Engineering
School of Industrial Engineering and Management
Royal Institute of Technology
SE-100 44 Stockholm
Sweden

ISBN 978-91-7729-843-4

献给我的家人

To my beloved family

Abstract

The martensitic microstructure with high defect density and supersaturated carbon can be considered a low-ductility microstructure. Thus, to improve its toughness it always undergoes a tempering treatment before it is put to use. During tempering, various secondary phases are precipitated within the matrix phase, and the evolution of these precipitate strongly influences the properties of martensitic steel, such as strength/ductility, fatigue, creep and hot corrosion resistance. Therefore, by controlling the precipitation phenomena many opportunities can open up for materials and process design optimization. Quantitative modelling of the precipitation phenomena is one path towards better control of the precipitation.

The Fe-C-Cr system forms the base system for important steel categories such as hot-work tool steels. They are characterized by high hardness and good toughness, even at elevated temperatures. In the present work, Fe-C-Cr model alloys were investigated to study precipitation in martensite during tempering. The as-quenched martensitic microstructures in these alloys with varying carbon and chromium content were systematically investigated using different experimental techniques. In addition, the evolution of the martensitic microstructure and precipitation during tempering was evaluated for two Fe-C-Cr alloys with low carbon content and varying chromium content using X-ray diffraction (XRD), electron backscatter diffraction (EBSD), electron channelling contrast imaging (ECCI) and transmission electron microscopy (TEM).

It was found that the morphology of fresh martensite and the ratio of high-angle grain boundary (HAGB) to low-angle grain boundary (LAGB) were affected by Cr addition, which is similar to the effect of C addition. However, the Cr addition had no effect on the micro-hardness whilst the C addition had a strong influence on it.

During tempering at 700 ℃, the coarse and fine laths of the as-quenched martensite coarsened slowly for both low carbon alloys. A clear difference between the two alloys was distinguished by studying structural units separated by high-angle boundaries (HABs). In the low-Cr alloy, M_3C precipitates formed and coarsened rapidly, thus they caused little hindrance for migration of HABs. In the high-Cr alloy, M_7C_3 precipitates formed and coarsened slowly, thereby providing a larger pinning effect on the HABs than that made by M_3C in the low-Cr alloy.

Then, a quantitative experimental characterization of the precipitates in the tempered martensite was performed. Moreover, the software TC-PRISMA, which is based on Langer-Schwartz theory and adopts the Kampmann-Wagner-Numerical (KWN) method, was applied to predict the precipitates formed in the Fe-0.15C-4.0Cr (mass%) model alloy after tempering. The important input parameters for the modelling were obtained from microstructure characterization of the as-quenched material. A careful comparison was made between the experimental results and the modelling predictions. The effect of parameters i.e., dislocation density, interfacial energy and grain size on the precipitates was discussed.

Furthermore, the growth and coarsening of precipitates in one of the model alloys: Fe-1C-1Cr (mass%) was studied with the help of electron microscopy analysis combined with DICTRA simulations. The chemical composition across the matrix-precipitate interface and within the precipitates was obtained for the 700 ℃ and 500 ℃-tempered samples. An apparent enrichment of Cr was found at the interface zone of precipitates after tempering at 700 ℃ for a short duration of 5 s, while such enrichment of Cr was found only after 30 min at 500 ℃, and in both cases the Cr/Fe ratio at the middle of the precipitate was equal to that in the matrix far away from any precipitates. The discrepancy between experimental data and calculations on the growth and coarsening of precipitates was discussed and then further development of the precipitation modelling was proposed.

Keywords Fe-C-Cr alloy; Microstructure; Precipitates; Tempering of martensite; Electron microscopy; Growth; Coarsening; Modelling.

Sammanfattning

Den martensitiska mikrostrukturen med hög defektdensitet och övermättad på kol kan betraktas som en mikrostruktur med låg duktilitet. För att förbättra segheten genomgår den oftast en anlöpningssbehandling innan den används. Under anlöpningen utskiljs olika sekundära faser inom matrisfasen. Utvecklingen av dessa utskiljningar påverkar starkt det martensitiska stålets egenskaper, såsom hållfasthet/duktilitet, utmattning, kryp och korrosionsbeständighet. Därför kan många möjligheter öppnas för material-och processoptimering genom att kontrollera utskiljningsfenomenen, t.ex. är kvantitativ modellering en väg mot bättre kontroll av utskiljningsreaktioner i martensitiska stål.

Fe-C-Cr-systemet utgör bassystemet för viktiga stålkategorier, såsom verktygsstål. De kännetecknas av hög hårdhet och bra seghet, även vid förhöjda temperaturer. I det aktuella arbetet undersöktes modell-legeringar av Fe-C-Cr med avseende på utskiljning i martensit under anlöpning. De släckta martensitiska mikrostrukturerna i dessa legeringar, med varierande kol- och krominnehåll, undersöktes systematiskt med användning av olika experimentella tekniker. Dessutom utvärderades utvecklingen av den martensitiska mikrostrukturen och utskiljningarna under anlöpning för två Fe-C-Cr-legeringar med lågt kolinnehåll och varierande krominnehåll med hjälp av röntgendiffraktion (XRD), ”electron backscatter diffraction” (EBSD), ”electron channeling constrast imaging” (ECCI) och transmissionselektronmikroskopi (TEM).

Man fann att morfologin hos färsk martensit och förhållandet mellan högvinkelkornsgränser (HAGB) och lågvinkelkornsgränser (LAGB) påverkades av Cr tillsats, vilket liknar effekten av C-tillsats. Men Cr-tillsatsen hade ingen effekt på mikrohårdheten medan C-tillsatsen hade ett starkt inflytande på den.

Under anlöpningen vid 700 °C förgrovades de grövre och fina lattorna hos den släckta martensiten långsamt för båda lågkol-legeringarna. En tydlig skillnad mellan de två legeringarna kunde observeras genom att studera strukturella enheter separerade av högvinkelgränser (HAB). I låg-Cr-legeringen utskiljs M_3C och förgrovas snabbt, och

orsakar sålunda ett litet hinder för rörelsen av HABs. I hög-Cr-legeringen utskiljs M_7C_3 som förgrovas långsamt, varigenom de ger en större pinning-effekt på HABs jämfört med M_3C i låg-Cr legeringen.

Därefter utfördes en kvantitativ experimentell karakterisering av utskiljningarna i den anlöpta martensiten. Dessutom användes mjukvaran TC-PRISMA, som är baserad på Langer-Schwartz-teorin med Kampmann-Wagners numeriska metod (KWN), för att förutsäga utskiljningarna som bildades i Fe-0.15C-4.0Cr (vikt%) efter härdning och anlöpning. De viktiga ingångsparametrarna för modelleringen erhölls från mikrostrukturkarakterisering av det släckta materialet. En noggrann jämförelse gjordes mellan experimentella resultat och förutsägelser från modelleringen. Effekten av olika parametrar, dvs dislokationstäthet, gränsenergi och kornstorlek på utskiljningarna diskuterades.

Vidare studerades tillväxten och sammansättningen hos utskiljningar i en modell-legering Fe-1C-1Cr (vikt%) med hjälp av elektronmikroskopianalys i kombination med DICTRA-simuleringar. Den kemiska sammansättningen över gränsytan matris/utskiljning och inom utskiljningarna erhölls för 700 °C och 500 °C-anlöpta prover. En tydlig anrikning av Cr hittades vid gränsytan efter anlöpning i 5 s vid 700 °C, medan en sådan anrikning av Cr fanns först efter 30 min vid 500 °C. I båda fallen var Cr / Fe-förhållandet vid mitten av utskiljningen lika med den i matrisen långt ifrån andra utskiljningar. Skillnaden mellan experimentella data och beräkningar på tillväxten och förgrovningen av utskiljningar diskuterades och förslag på utveckling av utskiljningsmodelleringen gavs.

Nyckelord Fe-C-Cr legering; Mikrostruktur; Utskiljning; Anlöpning av martensit; Elektronmikroskopi; Tillväxt; Förgrovning; Modellering.

Supplements

I. *Microstructure of martensite in Fe-C-Cr and its implications for modelling of carbide precipitation during tempering*

Ziyong Hou, Peter Hedström, Yunbo Xu, Di Wu and Joakim Odqvist.

ISIJ International, 2014, 51(11): 2649–2656.

II. *Quantitative modeling and experimental verification of carbide precipitation in a martensitic Fe-0.16 wt%C- 4.0 wt%Cr alloy*

Ziyong Hou, Peter Hedström, Qing Chen, Yunbo Xu, Di Wu and Joakim Odqvist. Calphad, 2016, 53:39–48.

III. *Microstructure evolution during tempering of martensitic Fe–C–Cr alloys at 700 ℃*

Ziyong Hou, R. Prasath Babu, Peter Hedström, and Joakim Odqvist.

Journal of Material Science, 2018, 53(9): 6939–6950.

IV. *Early stages of cementite precipitation during tempering of 1C-1Cr martensitic steel*

Ziyong Hou, R. Prasath Babu, Peter Hedström, and Joakim Odqvist.

Submitted manuscript.

V. *Coarsening of cementite during tempering of a martensitic steel*

Ziyong Hou, R. Prasath Babu, Peter Hedström, and Joakim Odqvist.

In manuscript.

The contributions by the author to the supplements of this thesis:

I. Supplement 1

Literature survey, sample preparation, experimental characterization, simulations, and writing of the first draft.

II. Supplement 2

Literature survey, sample preparation, experimental characterization, simulations, and writing of the first draft.

III. Supplement 3

Literature survey, sample preparation, experimental characterization, and writing of the first draft.

IV. Supplement 4

Literature survey, sample preparation, experimental characterization, simulations, and writing of the first draft.

V. Supplement 5

Literature survey, sample preparation, experimental characterization, simulations, and writing of the first draft.

Conference contributions (Oral presentation):

a) Adventures in the Physical Metallurgy of Steels, 23-25 July 2013, Christ's College. Cambridge UK.
b) The 2015 conference on Solid-Solid Phase Transformations in Inorganic Materials (2015 PTM) Whistler, BC, Canada, June 28 to July 3, 2015.
c) Silk Road International Symposium for Distinguished Young Scholars, Xi'an, China, 15-20 Nov, 2017.

Other contributions not included in this thesis:

A. *Effect of carbon content on the Curie temperature of WC-NiFe cemented carbides*
Ziyong Hou, David Linder, Peter Hedström, Annika Borgenstam, Erik Holmström, and Valter Ström.
Submitted manuscript.

B. *Enhanced grain growth behavior of ferritic steel during continuous cyclic annealing*
Ziyong Hou, R. Prasath Babu, Yunbo Xu, and Di Wu.
Steel Research International, 2018, DOI: 10.1002/srin.201800222

C. *Effect of holding temperature on microstructure and mechanical properties of high–strength multiphase steel*
Ziyong Hou, Di Wu, ShuXin Zheng, Xiaolong Yang, Zhuang Li, and Yunbo Xu.
Steel Research International, 2016, 87(9): 1203–1212.

Contents

Chapter 1 Introduction

1.1 Background

Steels are by far the most frequently used metallic material among a number of competitive materials [1]. The main reason for this is certainly their attractive properties e.g., strength and toughness, with a competitive cost and easy recycling [1, 2]. Moreover, the properties of steels can be manipulated over wide ranges by varying the chemical composition or processing parameters. Among various steel types, martensitic steels have been attracting attention due to their excellent combination of ultra-high strength as well as toughness, which can be improved by optimizing the heat treatments. This makes them amenable to metal forming operations and engineering machinery [1-5]. Historically, considerable efforts have been put into understanding steels from physical metallurgy view in order to improve the properties of martensitic steels, for example, by simultaneously increasing strength and toughness by nanoprecipitation [6-22]. Recent advances in theoretical and experimental analysis of iron-based alloys, induced by the development trend to integrated computational materials engineering (ICME) [23], enable more computationally-driven design and optimization of tempered martensite. To further improve the development of advanced steels with high production efficiency and low cost, a fundamental understanding of the precipitation reaction, including the growth and coarsening mechanisms and their contribution to the microstructure during tempering, is still needed [1, 3, 24, 25].

Upon tempering, the coarsening of martensitic microstructures occurs. Accompanying the microstructure changes, various new phases may also precipitate during tempering [1-4]. Thus, the mechanical properties of tempered steels, such as hardness, would also change due to its strong relationship with the microstructure. On one hand, several factors including recovery of dislocation structures and recrystallization, annihilation of low

angle grain boundaries, migration of interstitial atoms from body centered cubic (BCC) or body centered tetragonal (BCT)- iron structure, decomposition of retained austenite, precipitation and coarsening of the precipitates, may lead to softening of the matrix phase [1, 3, 4]. In an alternative but often simultaneous scenario, if strong carbide forming alloying elements are added and proper tempering is employed, the formation of densely dispersed precipitates coherent with the matrix phase may result in an increase in both strength and ductility [7-14]. Hence, the properties of martensitic steels are determined by the tempered martensitic microstructure i.e., both the matrix phase and the new precipitated second phase(s). Understanding of the precipitation reaction by advanced experimental and computational methodology is thus required for advanced material design and optimization of heat treatments [1, 3, 24, 25].

In the past decades, substantial research on the precipitation and the accompanied microstructure evolution in martensitic steels during tempering has been conducted using various characterization methodologies [3, 26, 27]. Chemical composition at and across the precipitates/matrix interface is a way to indicate the interface migration conditions during the nucleation and growth of the precipitates [5, 25]. Thus, chemical analysis at local zones is required in order to understand the precipitation reaction further. In addition, the interaction between the microstructure and the precipitates during tempering still needs to be better understood, e.g., which type of boundaries or structures will be effectively pinned by the precipitates, how the dislocations change depending on the tempering time and temperature and the mechanism of lath boundaries merging or migration [3, 28-32]. Beside the above-mentioned experimental studies on the precipitation, developed models implemented in commercial software packages that consider different assumptions have also been used to simulate the precipitation process in different materials based on the thermodynamic database [33-52]. However, the investigation of precipitation in martensite during tempering is often performed on a qualitative or semi-quantitative basis, and few quantitative studies have been performed [25, 49, 52]. To take advantage of the precipitation in tempered martensite, the thermodynamic and kinetics behavior of precipitation needs to be better understood.

1.2 Scope of the present work

The major goal of the present thesis is to quantitatively characterize and model the precipitation during tempering of martensitic Fe-C-Cr steels. Therefore, different investigations have been carried out:

(1) First, the fresh martensitic microstructure in four Fe-C-Cr steels was well characterized to refine and further understand the influence of elements Cr and C on the martensitic microstructures. Based on that, the microstructural parameters were used as input for the precipitation modelling to increase knowledge of the initial microstructure's role on the precipitation during tempering. (Paper I)

(2) Second, precipitation kinetic simulations including nucleation, growth and coarsening were carried out. The comparison between experimental data and simulations provide a basis for further refinement of the modelling. (Paper II)

(3) Third, microstructure evolution during tempering was systematically characterized. The discussion of the interaction between the precipitates and martensitic microstructure gives an insight to the correlative evolution of microstructure and precipitation during tempering, and maybe considerations for the refinement of the modelling of precipitation. (Paper III)

(4) Fourth, the chemical composition across the precipitate/matrix interface was evaluated by both experiments and calculations, aiming to further increase understanding of the controlling mechanism at the phase interface during early stages of precipitation of M_3C. (Paper IV)

(5) Fifth, the coarsening of precipitates in martensite during tempering was studied by comparing experiments and kinetic calculations, and the mean size and particle size distribution of M_3C precipitates in martensitic steel were discussed, again in order to extend the capability of modelling. (Paper V)

Chapter 2 Martensite

2.1 Martensite transformation

The name “martensite” was coined to honour Adolf Martens for his metallographic observations in 1890 [1, 5]. Originally, it was used to describe the hard phase found in quenched steels. Nowadays, it has been extended to designate any diffusionless product in e.g., ferrous, nonferrous, ceramics, and minerals during either cooling or deformation [1, 4, 5, 53, 54].

Martensite transformation in steels mostly occurs during rapid cooling from above austenitic temperature, which is also referred to as quenching, during which the cooling rate is sufficient to avoid any diffusional solid-state transformations, e.g., ferrite and pearlite [1, 3, 53-55]. Depending on the carbon and alloying elements content, the martensite transformation may be partially or fully completed at room temperature. Hardenability is the ability of steel to form martensite on quenching, which also indicates the criterion cooling rate needed for a martensitic transformation to occur.

During martensitic phase transformation in steels, the austenite with a face-centered cubic (FCC) lattice is transformed to martensite with a body-centered tetragonal (BCT) lattice by a diffusionless shear process [53-54]. Due to the large difference in alloying solubility between FCC lattice and BCT lattice, the distorted BCT lattice will be highly supersaturated with carbon [1]. A linear relationship between the lattice parameter *a* and *c* of BCT martensite has been established for plain carbon steels [56, 57]:

$$c/a = 1 + 0.045 wt\%C \tag{2.1}$$

Therefore, the carbon content in the matrix could be evaluated by calculating the lattice parameters using sophisticated experiments [55-58]. Nevertheless, the martensite can be

approximately considered as a body-centered cubic (BCC) lattice structure when the carbon content is very low.

2.2 Martensitic microstructure

Depending on, e.g., chemical composition, cooling rate and degree of under-cooling, the martensitic microstructure as well as its mechanical properties of steel always vary [21-23, 51, 59-66]. Furthermore, the evolution of martensitic microstructures during tempering or service is strongly related to the initial microstructure [24, 58]. Thus, characterization of the martensitic microstructure in both initial and tempered conditions is crucial for improving our understanding of martensite.

Until now, to describe various microstructure of martensite, several nomenclatures have been developed and used based on its morphology such as lath, plate, butterfly, lenticular and thin plate [1, 2, 24]. Fig. 2.1 shows a schematic of morphologies and martensite start temperature (M_s) changes with carbon content in binary Fe-C alloys [2]. In principle, an increase in carbon content permits the gradual transition from lath to plate. While, a mixture of martensitic microstructures, i.e., lath and plate, is often found in most practical cases due to the transition of martensite morphology occurring during the whole composition range of carbon.

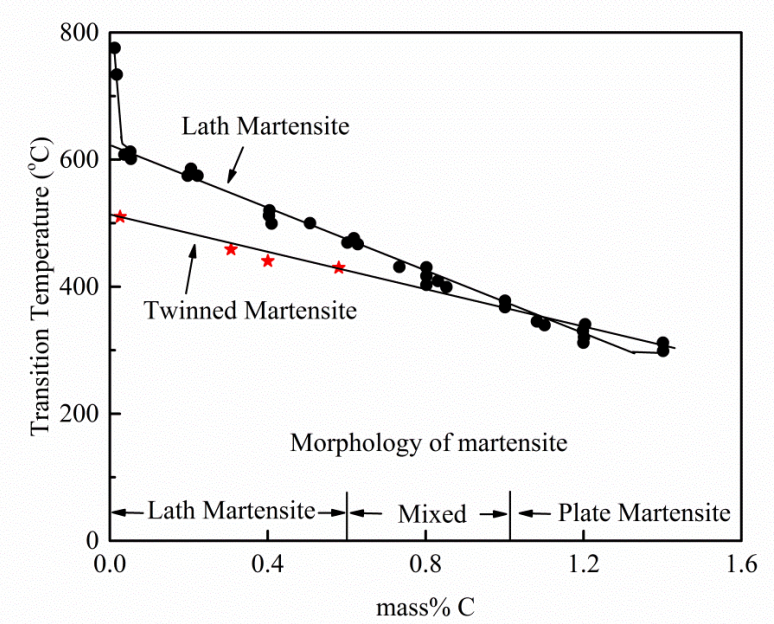

Fig.2.1 Martensite morphology along with martensite start temperature (M_s) as a function of carbon content in Fe-C alloys [2].

Furthermore, in alloyed steels, the martensitic microstructure is affected by the addition of alloying elements. The fundamental point of the morphology change in martensite is dependent on its preferred type of plastic deformation, which is determined by the critical resolved shear stress (CRSS) for slip and twinning at the transformation temperature [1, 2, 14, 51]. Alloying elements, with the exception of Co, will decrease the M_s temperature and increase the twinning slip tendency. Fig. 2.2 represents examples of the light optical microscopy (LOM) microstructure of as-quenched Fe-C-Cr alloys [51, 64].

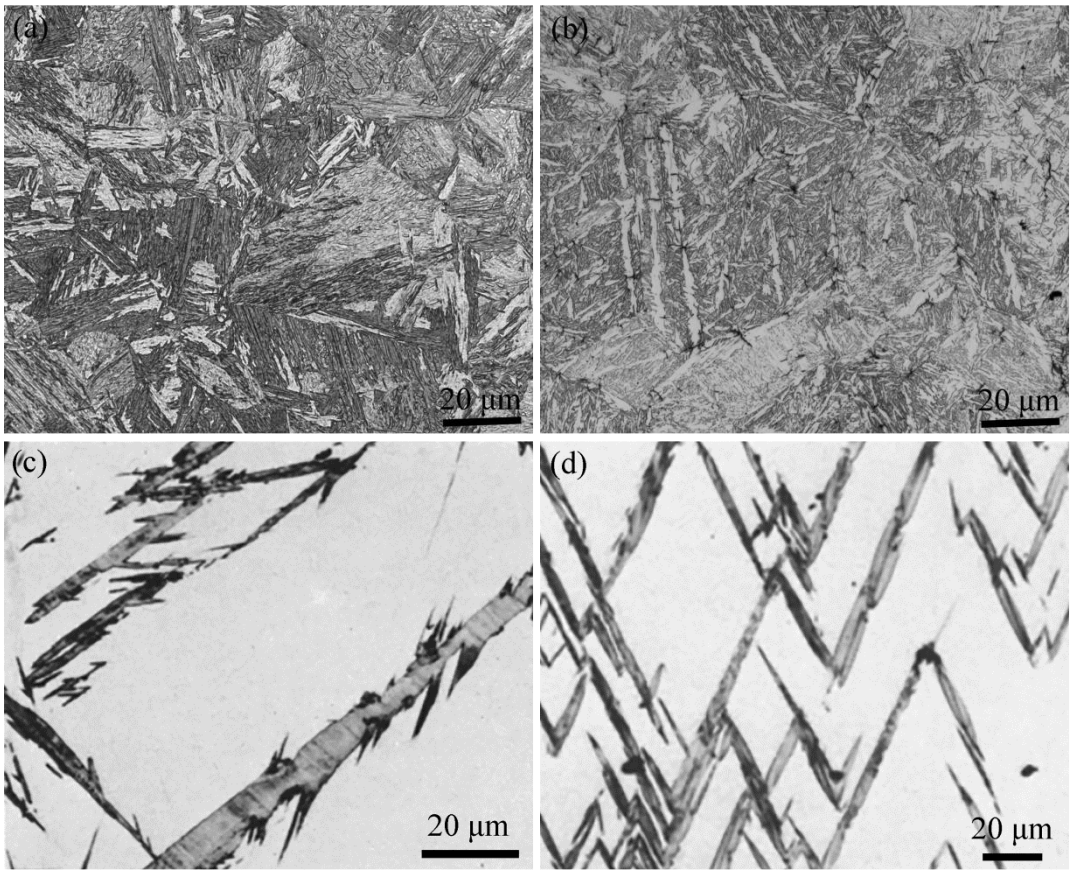

Fig. 2.2 LOM images of martensitic microstructure in ternary Fe-C-Cr alloys.
(a) Fe-0.15C-1.0Cr (mass%), lath martensite, (b) Fe-1C-4Cr (mass%), plate martensite after austenitizing at 1100 ℃ for 10 min, followed by quenching in brine to room temperature, Images are from [51].
(c) Fe-1.44C-3Cr (mass%), (d) Fe-0.92C-8Cr (mass%), thin plate martensite, after austenitizing at 1150 ℃ for 30 min, followed by quenching in brine to 0 ℃ and 30 ℃. Images are modified from [64].

Martensite can be considered as a complicated hierarchical structure with high defect density. In the hierarchical martensite, units with heterogeneous composition and hardness assemble in a specific way, decided by factors such as which way the maximum strain or stress could be relieved during the martensitic phase transformation upon quenching [61, 67-72]. In Fig. 2.3, a schematic of substructure in lath martensite [70], which is mostly found in low-carbon and low-alloyed steels with high M_s temperature, is

presented. The hierarchic units in martensite have the following order from large to small: prior austenite grain - packet- block- (sub-block) – lath. The length-scales of these hierarchic structures range from several hundred micrometers to several tens of nanometers [72]. In addition, a high density of dislocations (10^{14}–10^{16} m^{-2}) arranged inside and at the boundaries of laths is one of the obvious features in lath martensite [60, 73]. Since lath martensite usually has a superior combination of toughness and strength, it is the most common constituent in high-strength steels. While, the plate martensite is usually found in high-carbon and high-alloyed steels with low M_s temperatures, and consists of coarse plates with or without mid-rib and planar defects [74, 75].

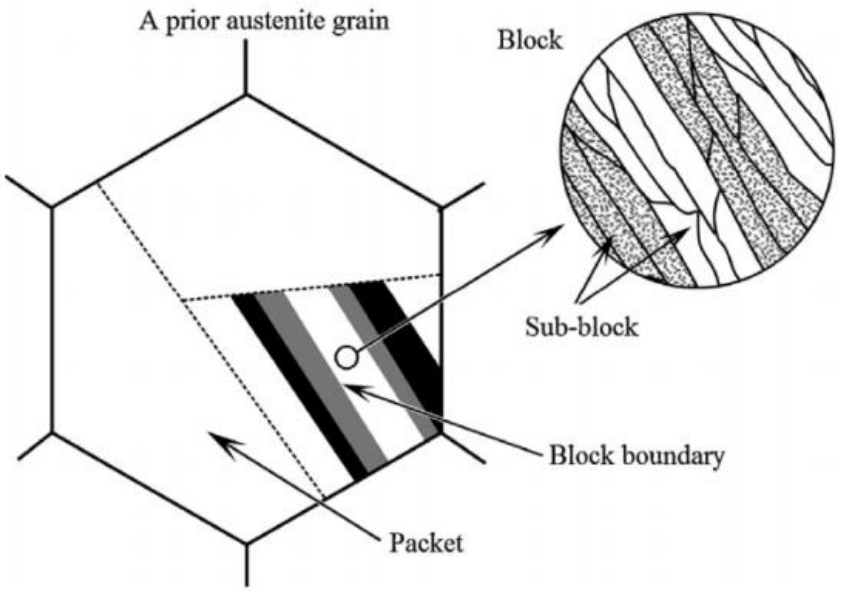

Fig. 2.3 Schematic drawing of hierarchical microstructure for lath martensite [70].

The features of martensite such as dislocation density, grain boundaries distribution and size of various units, provide the primary information on e.g., nucleation sites for precipitation.

2.3 Tempering of martensite

To achieve the desired hardness, strength, ductility or toughness, martensitic steels are often subjected to tempering after quenching [1-5]. Tempering essentially involves

heating the material to elevated temperatures in the range of between 150 and 700 ^{o}C, which is below the Ac_1 temperature (austenite start temperature), and holding for a specific time [1]. In some cases, double or multiple tempering instead of single tempering is performed for martensitic steels, for example, eliminate fresh martensite and austenite [4].

In recent decades, optimization of tempering parameters including tempering temperature and time, heating rate, etc., has been studied intensively to improve the mechanical properties [4, 6, 10-11, 15-23]. Depending on the chemical composition and the required mechanical properties for the martensitic steels, the selection of tempering parameters varies considerable. In the case of hot-work tool steels, the tempering temperatures are mostly in the range of from 500 ℃ to 650 ℃, even up to 700 ℃. At this tempering temperature, precipitation of various secondary phases is promoted by the increased diffusivities of carbides-forming alloying elements [1, 4].

Depending on the tempering temperature and time, the evolution of microstructure in martensitic steels may vary significantly during tempering. At tempering temperatures below 250 ℃, interstitial atoms such as carbon are mobile but the substitutional elements are almost immobile due to their very low diffusivities [1]. Thus, carbon plays a dominant role in the transition carbide formation at low temperature tempering [76]. At tempering temperatures between 250 to 450 ℃, further carbon released from the matrix enable the formation of cementite, and the stable cementite and ferrite will replace the transition carbides and low-carbon martensite [1]. With the tempering temperature increasing up to 700 ℃, sufficient thermal energy is available for substitutional elements to be mobile and influence the microstructural coarsening [1]. Fig. 2.4 shows a tempered martensite in Fe-0.15C-1Cr (mass%) alloy. After being tempered at 700 ℃ for 1000 h, the lath-shaped martensite is transformed to polygonal ferrite with large precipitates. After being tempered at 500 ℃ for 1000 h, the lath-shaped martensite can still be observed.

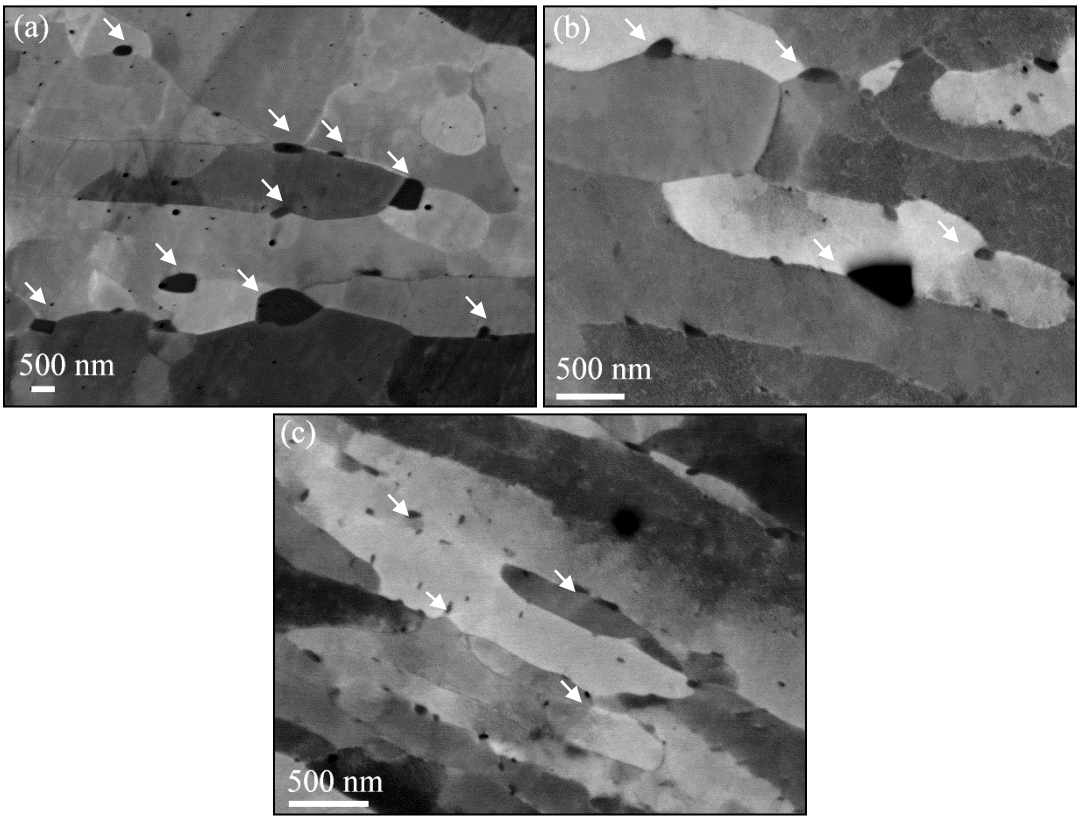

Fig. 2.4 SEM-ECCI microstructure of Fe-0.15C-1.0Cr (mass%) alloy after tempering at: (a) 700 ℃; (b) 600 ℃; (c) 500 ℃ for 1000 h. White arrows represent precipitates.

In addition to the influence of tempering temperature and time, the martensitic microstructure evolution during tempering is also dependent on its chemical composition. During tempering the fine dispersed precipitates can retard the migration of various defects such as boundaries and dislocations, resulting in a different coarsening rate of the martensitic substructure, see Fig. 2.5. On the other hand, the interaction between the formed precipitates and various boundaries may also affect either recrystallization or recovery behavior in tempering martensite [3, 29-32].

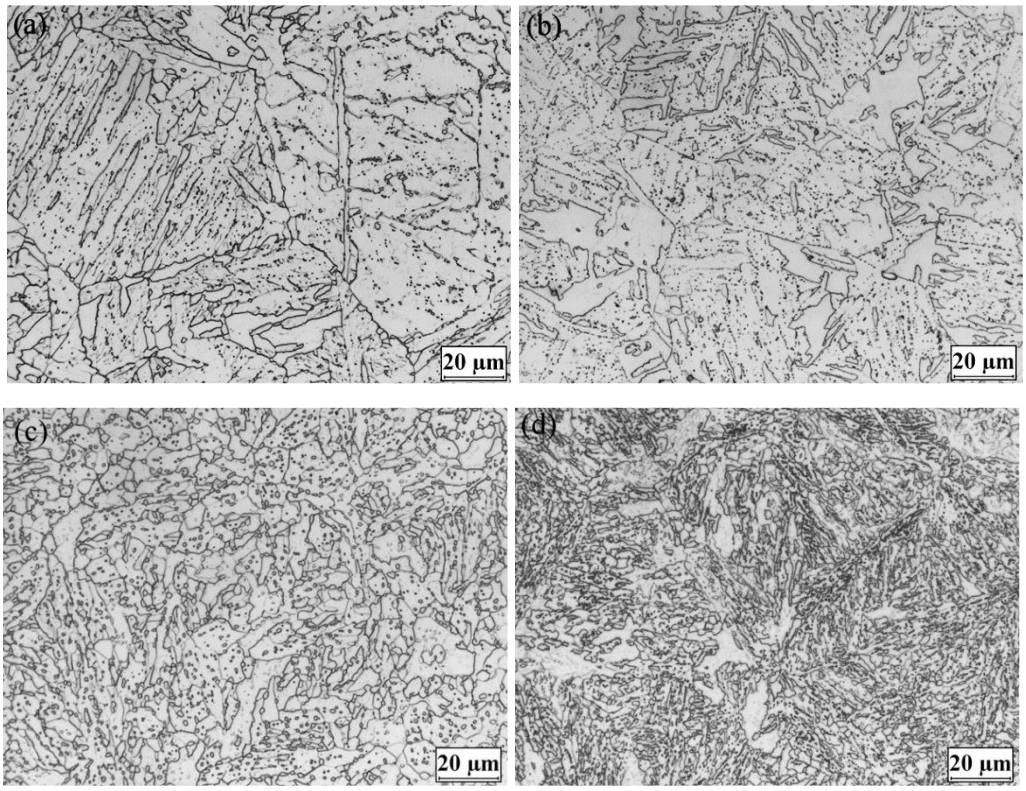

Fig. 2.5 LOM microstructure of alloys: (a) Fe-0.15C-1.0Cr; (b) Fe-0.15C-4.0Cr; (c) Fe-1C-1Cr; (d) Fe-1C-4Cr. after tempering at 700 ℃ for 1000 h. Black points are precipitates, black curved lines are boundaries, grey blocks are the matrix phase.

The coarsening of martensitic microstructure during tempering results in different length scales, ranging from the characteristic diffusion length of interstitial or substantial atoms to movement of grain boundaries distance, within an overlap in temperature and time range. Thereby, fully characterizing this hierarchical martensite evolution during tempering remains a challenge.

The variation of chemical composition, quantified by the state-of-the-art experimental techniques, at and far away from the interface of the precipitated phase and parent phase during tempering could indicate the nucleation and growth controlling mechanism of precipitates [37, 38, 76]. The interplay between microstructure and precipitation is also essential to obtain an understanding of the microstructure evolution during tempering.

Thus, characterization of tempering microstructure is needed and can be used to refine and extend the applicability of the existing modelling [37].

Chapter 3 Precipitation

Precipitation reaction is one type of phase transformation during which fine size second-phase particles nucleate and grow from a parent phase [25, 77]. This reaction can be found in many materials, such as Cu-Zn, Al-Mg and steels, during different processes including aging, annealing and tempering etc.

3.1 Stages of precipitation evolution

Precipitation often occurs when the concentration of interstitial and substitutional elements exceed their solubility in an alloying system. In the precipitation reaction, the driving force is provided by the chemical potential gradient, which is directly proportional to the composition difference in the initial and the equilibrium state. In addition to the dependence on the chemical composition and temperature, the precipitation process is also strongly affected by duration time, which is called kinetics [25, 78]. Due to the kinetics of precipitation, a precipitation reaction has its own nucleation sequence [25, 76-78].

The evolution (includes spatial and temporal) of the precipitation during treatment is determined by the composition, tempering parameters and initial microstructure of the parent phase [25, 49, 79]. The precipitation process can be divided in three stages, i.e., nucleation, growth and coarsening, in principle [25]. In Fig. 3.1, a schematic of the precipitation process is presented. It is worth mentioning that, in reality, prior to the precipitation, the supersaturated atoms are not homogeneously distributed in the bulk alloy, they may segregate at the place where plenty of defects (dislocations and boundaries in martensitic steels) are present [56, 57, 67].

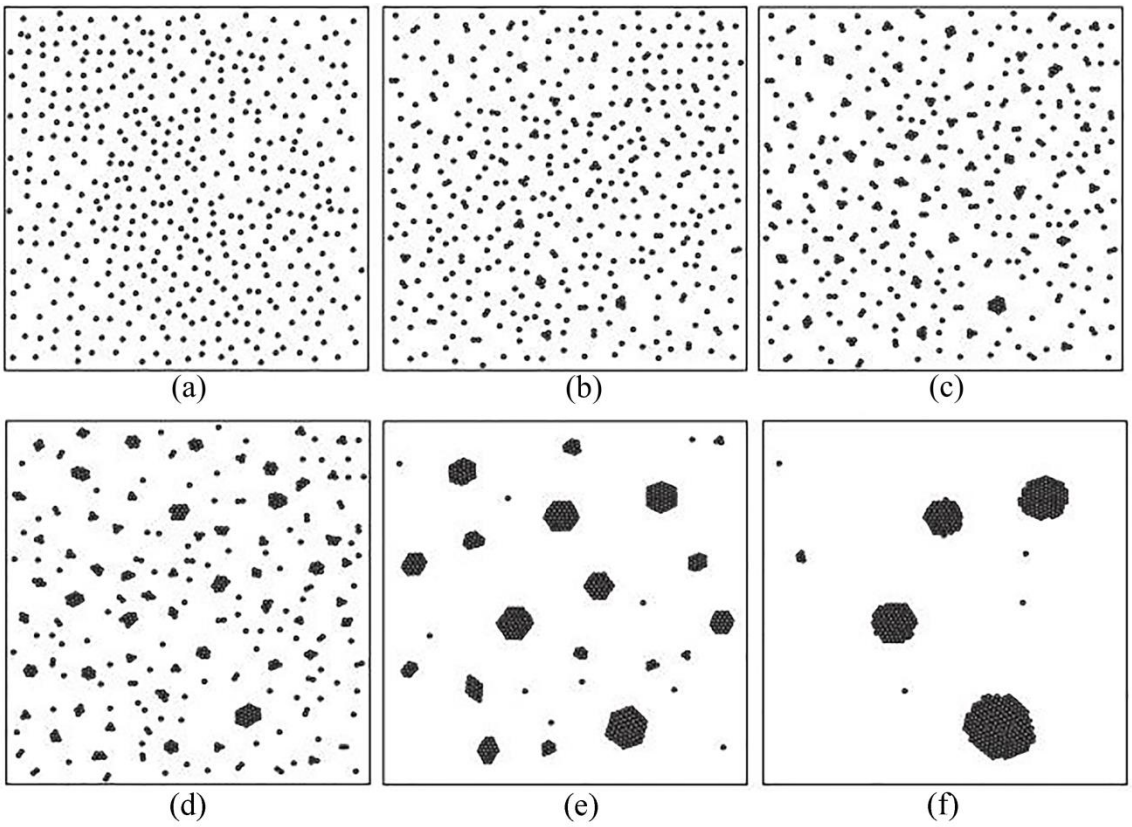

Fig.3.1 Schematic of the precipitation progress.

(a) random solution; (b) equilibrated solution; (c) nucleation-growth; (d) growth and coarsening; (e-f) coarsening. Images are from [25].

In the nucleation stage of precipitation, the spatial fluctuation of the phase structure and concentration is developed within a supersaturated metastable alloy. From the modelling perspective, when a spherical nucleus is formed, the change in Gibbs free energy is given by the following terms [25, 48-50, 77]:

$$\Delta G = \frac{4}{3}\pi (r^i)^3 (\Delta G_v + \Delta G_{st}) + 4\pi (r^i)^2 \gamma \tag{3.1}$$

where r^i is the radius of the spherical embryo, ΔG_v is the chemical free energy change per unit volume of embryo, ΔG_{st} is the strain energy per unit volume of embryo due to misfit between the nuclei and matrix, and γ is the interfacial energy between the nuclei and matrix. The first term in Eq.3.1 is the specific volume free energy change, while the

second term is the energy needed to form a unit area of precipitate-matrix phase interface. The change of ΔG is dependent on the two opposite contributions from the two terms in Eq.3.1. Thus, there will be a maximum ΔG at a critical radius r^*. In the case with a maximum ΔG, the ΔG decreases with increasing size only above a critical radius r^*. The critical radius and critical energy for the nucleus can be written as follows [25, 48-50, 77]:

$$r^* = -\frac{2\gamma}{\Delta G_v + \Delta G_{st}} \tag{3.2}$$

$$\Delta G^* = -\frac{16\pi}{3}\frac{\gamma^3}{(\Delta G_v + \Delta G_{st})^2} \tag{3.3}$$

The critical nucleation energy ΔG^* is the key parameter for evaluating the steady nucleation rate in solid materials. The nucleation process is always considered as a "stochastic" process since it occurs with a certain probability. Therefore, the nucleation rate should always be treated in a statistical framework, it is meaningless to say whether a single nucleus will appear exactly at a certain situation [77].

When a nucleus has reached a supercritical size ($r > r^*$), the nucleus grows in nature through adsorption of additional precipitate-forming atoms-the atoms prefer to bond together and form a more stable phase as it proceeds to the growth stage. Whereas it may be dissolved when the nucleus is smaller than a critical size ($r < r^*$).

During the growth of nucleated precipitates, the concentration of supersaturated atoms in the matrix will decrease, and which in the precipitate will approach to the equilibrium condition. Generally, the growth stage continues until the equilibrium fraction of the new precipitated phases has been reached, where an energetic equilibrium has been achieved between the amount of alloying elements in the precipitates and in the matrix. Thereafter, the coarsening of precipitates commences where larger particles grow and smaller particles dissolve. The coarsening process is also called Ostwald ripening [80-81], which

is driven by curvature-induced pressure as referred to as the Gibbs-Thomson effect [25, 47, 80, 81].

Fig. 3.2 gives the parameters, including mean size, volume fraction and nucleation sites of precipitation at these three stages. The experimental information, such as the correlation between the mean size of precipitation and tempering time, indicates the controlling mechanism at different stages of precipitation [3].

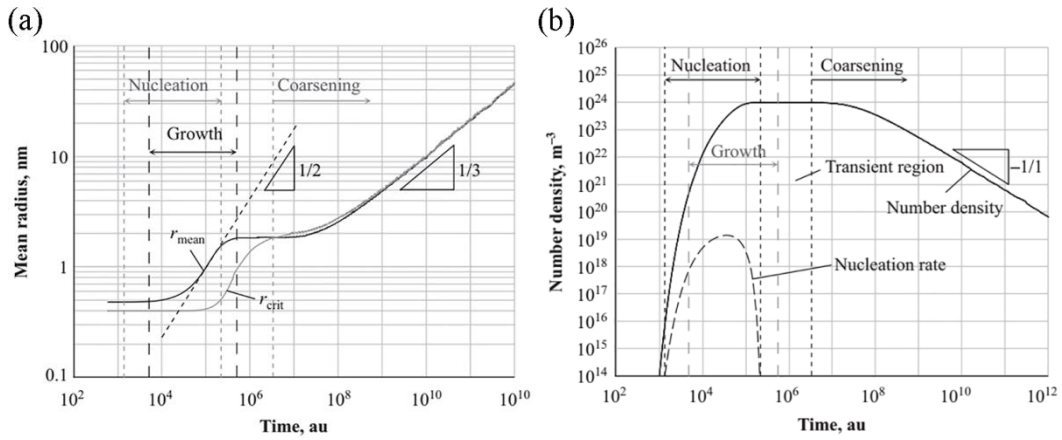

Fig. 3.2 Evolution of precipitation parameters: (a) mean radius/critical radius and (b) number density/nucleation rate. Images are from [77].

The three above-mentioned stages of precipitation often overlap each other [84]. Thus, in many recently developed models the precipitation process is considered as a concurrent process, i.e., the transition between each stage is captured automatically [49].

3.2 Types of precipitates in steels

Precipitates in steels could be intermetallic phases, oxides, sulphides, nitrides and carbides, etc. [83]. In the present work, carbide precipitation is exclusively dealt with considering their strong relationship with the mechanical properties in Fe-C-Cr alloys.

Over the past few decades, considerable research has been devoted to characterizing the precipitation during tempering of steels including identification and quantification using various sophisticated experimental methodologies [76, 84-87]. Cementite (Fe_3C) often

forms during tempering in plain carbon steels. While in alloyed steels, several types of precipitates, such as MC, M_2C, M_3C, M_7C_3, $M_{23}C_6$ and M_6C, may precipitate during tempering.

Several classical types of precipitates in Fe-C-Cr alloys are listed in Table 3.1. The lattice parameters given in Table.3.1 all represent for precipitates with the exact composition. It can be seen clearly from Table.3.1 that the crystal structure and compositions differ considerably between different types of carbides. The chemical composition of precipitates always approaches the equilibrium value with the tempering time prolonged, and this can result in variation in the structure parameters of precipitates due to differences between each type element in the lattice parameter. Thus, changing of the structure parameters of precipitates can indicate variations in the chemical composition during the precipitation process.

Table 3.1 Typical carbon precipitates in Fe-C-Cr alloys [83].

Carbide	Crystal system	Fe or M/C ratio
ε	Hexagonal a=2.735 c =4.339Å	2.4-3.0
η	Orthorhombic a=4.704 b=4.318 c =2.830Å	2
MC	Faceted cubic a=2.830Å	1
Fe_3C	Orthorhombic Pnma a=4.525 b=5.087 c =6.743Å	3
$M_{23}C_6$	Cubic F Fm-3m a =10.621Å	23/6
M_7C_3	Orthorhombic Pnma a=4.526 b=7.010 c =12.142Å	7/3

3.3 Precipitation in martensitic steels

Precipitation in tempered martensite occurs in various forms. The precipitation in martensite may go through the following steps: segregation of carbon atoms to dislocations and boundaries, rearrangement and clustering of carbon atoms, formation of transient carbides and decomposition of retained austenite (if there is any), formation and coarsening of more stable carbides at the expense of transient carbides.

Unlike in recrystallized polygonal ferrite or austenite, the martensitic microstructure has an extraordinarily complex environment for the precipitation, especially for the nucleation and growth stages. First, as it has a heterogeneous composition and microstructure in the as-quenched martensite due to the phase transformation sequence [67-68], segregation of atoms can occur at dislocations and boundaries. Second, the hierarchical martensitic microstructure could lead to multiple nucleation sites. Comparing with the precipitation in other low temperature microstructure, for instance precipitation in banite, the supersaturation and dislocation density in martenstie are often higher than these in bainites. Furthermore, the interplay of the precipitation and supersaturated matrix phase in martensite during tempering also influences the precipitation reaction. Fig. 3.3 shows the precipitates in martensitic Fe-C-Cr alloys after being tempered at 700 ℃ for 5 s. The size and shape of precipitates vary a lot due to the initial martensitic structures and composition.

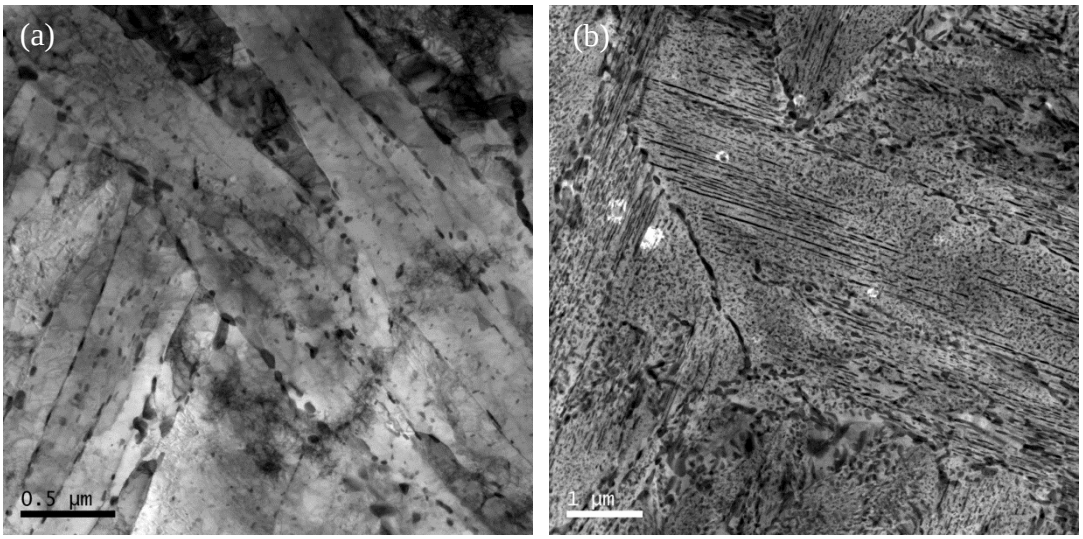

Fig. 3.3 Precipitates in martensitic Fe-C-Cr alloys during tempering
(a) Fe-0.15C-1.0Cr alloy; (b) Fe-1C-1Cr alloy, austenitizing at 1100 ℃, followed by quenching in brine and tempering at 700 ℃ for 5 s.

In martensitic steels, the boundaries between two neighbor grains or crystallites are usually categorized into low-angle grain boundaries (LAGBs) and high-angle grain boundaries (HAGBs) by setting a criterion misorientation angle, 10 to 15^{o} [55, 70]. Each type of boundary has its own features, for example, HAGB has a higher energy in general than a LAGB. Hence, a low nucleation barrier energy is needed to overcome this in order to form the nucleus [25, 88]. This is one probable reason that the precipitates always prefer to nucleate at HAGBs. Fig. 3.4 shows TEM bright field images for the precipitates in a Fe-0.15C-4.0Cr alloy after tempering at 700 ℃ for 30 min. It is clear that the precipitates form at lath boundaries as well as inside laths. Meanwhile, different sizes of precipitates can be recognized between ones formed at boundaries and those formed at intra-lath.

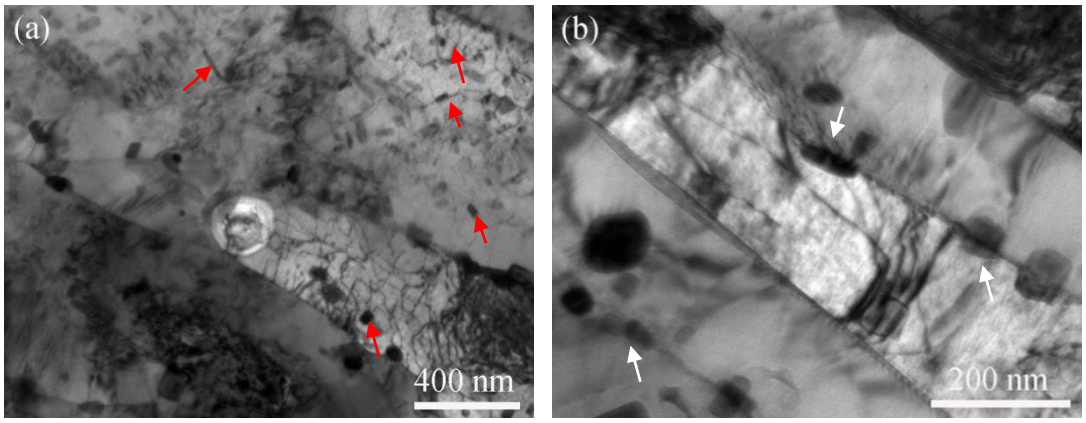

Fig.3.4 Precipitates form inside of laths: matrix and dislocations (a) and at boundary (b) in a martensitic Fe-0.15C-4.0Cr alloy after tempering at 700 ℃ for 30min. Red arrows: dislocation and intra- lath, White arrows: precipitates at boundaries. Images are from [52].

Since growth and coarsening of precipitates are a diffusion-controlled process, the diffusion rate of each element becomes a key parameter for evaluating the evolution of precipitates in a certain alloy system. Fig. 3.5 shows the ratio of diffusivity of some elements between the grain boundaries or dislocations and the bulk. The ratio between bulk and heterogeneous diffusion paths shows that grain boundary and dislocation diffusion are several to tens of orders larger than that in bulk. At a typical tempering temperature for martensitic steels, the ratio of diffusivity at grain boundaries or dislocations to that of the bulk is at least 10^5 to 10^9. The ratio at low temperature, e.g., 300 ℃, reaches several tens order of magnitude, which indicates that in practice diffusion at low temperatures will occur only along the boundaries and dislocations. Thus, the influence of defects on the diffusivity of each element should be considered when modelling the precipitation in martensitic steels during tempering.

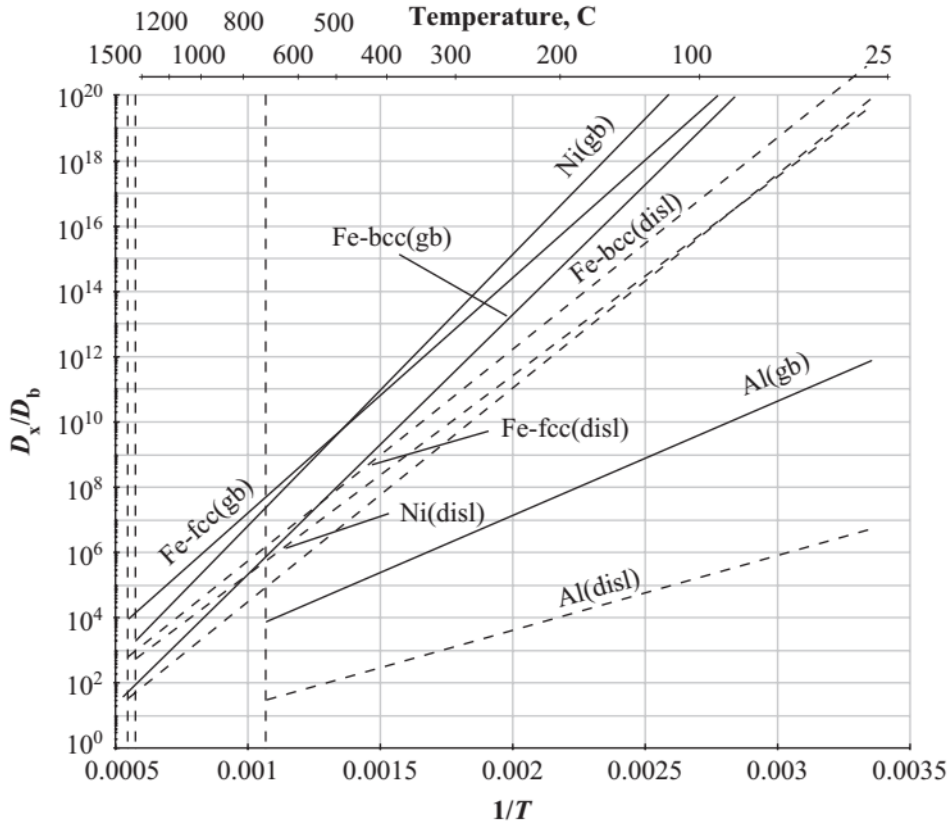

Fig. 3.5 Ratio between bulk and grain boundary (gb)/dislocation (disl) self-diffusion for Fe, Al, and Ni. Image is from [88].

Large size precipitates will still be at grain boundary in martensite after tempering. Fig.3.6 shows EBSD maps of the phase map and grain boundaries. Precipitates located at grain boundaries are the domain feature after tempering. Fig. 3.6 reveals that grain boundary is still important for the late growth and coarsening stage. Therefore, study of boundary distribution of martensite at both early and late stages of precipitation is necessary to understand the precipitation evolution during tempering.

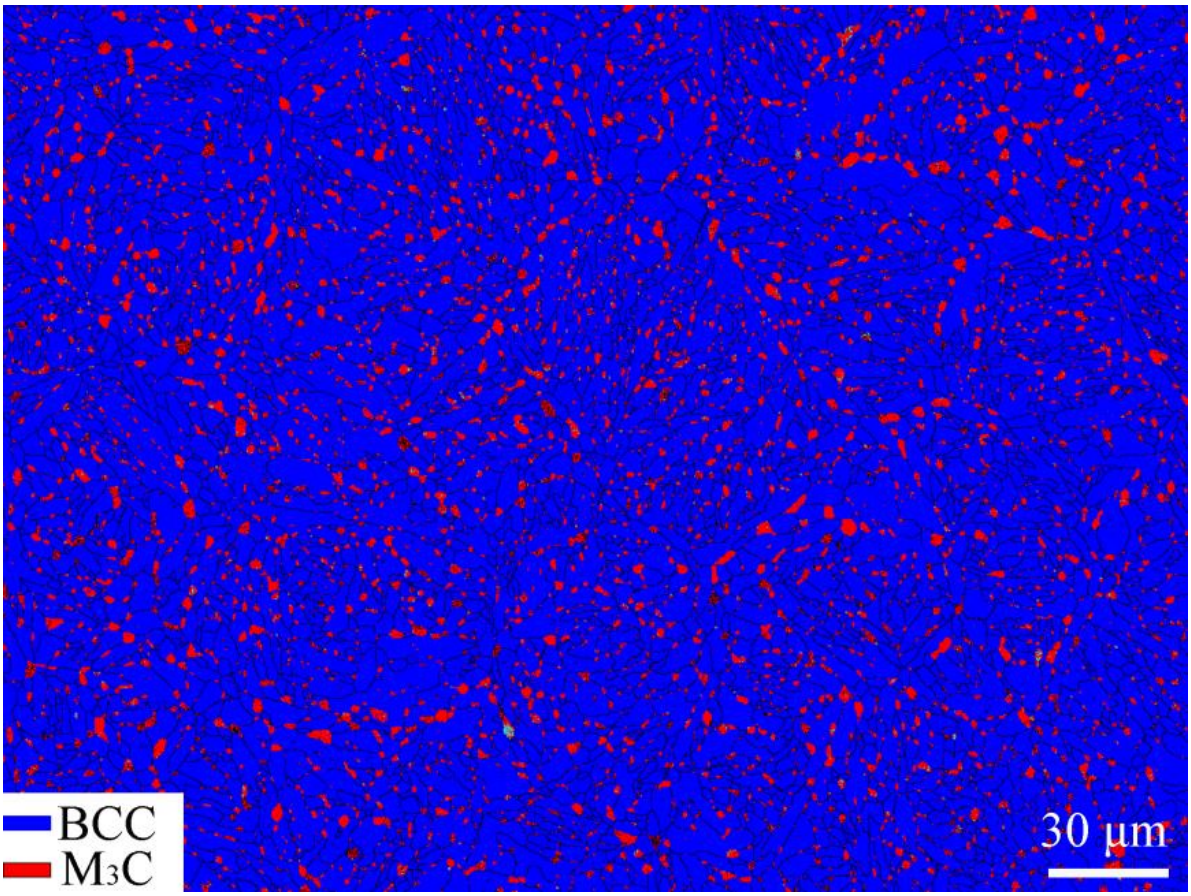

Fig. 3.6 Precipitates at grain boundaries in Fe-1C-1Cr alloy after tempering at 700 ^{o}C for 5000 h. Red: precipitates, blue: ferrite, black lines: boundaries with misorientation angle larger than 10^{o}.

Chapter 4 Thermodynamic and Kinetic Modelling

Thermodynamic and kinetic modelling have been used as very powerful tools for materials design and development [33, 53]. In this chapter, some aspects of this kind of modelling are briefly outlined. Special attention is paid to thermodynamic modelling (Thermo-Calc) [89] and kinetic modelling (TC-PRISMA and DICTRA) [90, 91], which have been used in the present work (see Papers I, II, IV and V) [37, 38, 51, 52].

4.1 Aim of modelling

The traditional way to design new advanced materials is based on metallurgical experience gained through numerous trial and error experiments. In some cases, a relatively long process time and the amount of cut-down materials for test will lead to a huge cost, e.g., a creep test may need ten years. On the other hand, extrapolation of the available experimental data to unknown regions, e.g., ultra-short term or long-term heat treatments, low temperature, is usually unreliable since the variation of physical parameters always varies with time.

Thus, there is a need to reduce the empiricism and extensive testing by increasing understanding of the physical mechanisms from prior experience. The idea here is to predict e.g., the evolution of precipitates and the matrix phase during tempering of martensite, given the initial microstructure, composition and tempering conditions. Therefore, a reliable integrated model, which can potentially simulate both the evolution of the initial microstructure and its corresponding mechanical properties during tempering would be favorable in alloy development.

4.2 Thermo-Calc

The Thermo-Calc software package (originally developed at the KTH Royal Institute of Technology in Stockholm) is commonly used for equilibrium calculation by many research institutes and industries. The equilibrium information for each phase at certain conditions (temperature, pressure, volume, chemical composition) can be illustrated in a phase diagram, where thermodynamically distinct phases coexist at equilibrium conditions [33, 92]. Fig. 4.1 shows two sections from phase diagrams for Fe-C-Cr alloys. The additional information e.g., fraction, constituents, is also available.

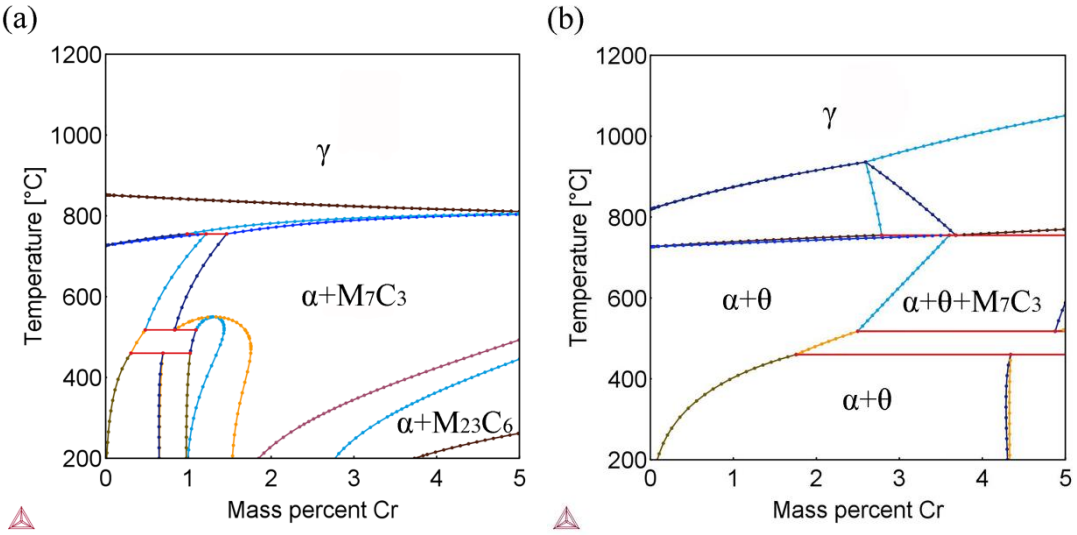

Fig. 4.1 Phase diagram of Fe-C-Cr alloys with 0.15C (a) and 1.0C (mass%) (b), γ represents austenite; α represents ferrite, θ represents cementite. Software Thermo-Calc with TCFE9 database has been used.

Not being limited to binary or ternary alloys, it is possible to extend the thermodynamic modelling to predict the phase behavior in multi-component materials based on the extrapolation of properties from their lower-order systems to higher-order systems [92]. This significantly extends its application field of modelling for designing real alloys since in practice one alloy often contains several components. Furthermore, valuable information for heat treatments can be obtained from the phase diagram, e.g., austenite temperature, tempering temperature to get the required phase.

4.3 Kinetic modelling

To understand and model the materials behavior in conditions far from thermodynamic equilibrium, the kinetic model is developed to include fundamental models to critically assess the thermodynamic and kinetic data [90, 91]. DICTRA and TC-PRISMA are two software programmes used for simulating the precipitation behavior in, for example, martensitic steels during tempering [41-46]. In software DICTRA, several assumptions at the interface are implemented, e.g., the movement of a phase interface is controlled by the mass balance obtained from the fluxes of the diffusing elements across the interface, and local equilibrium is assumed at the moving interface [90, 92]. The details of the assumptions and concepts of modelling implemented in the present software can be found elsewhere [40, 41, 48, 92].

Compared to TC-PRISMA, with DICTRA one can in practice only perform simulations with a limited number of particles, while TC-PRISMA enables quantitative modelling of thousands of particles in multicomponent systems and also treats all three stages of precipitation like a concurrent stage [48, 91]. Hence, DICTRA is quite suitable when studying the specific interface conditions, for example, composition versus distance to the interface under different growth model settings, such as PE or NPLE, and even in some case the size evolution (and volume fraction) agrees well with the experiments [50]. The results calculated by TC-PRISMA can be compared quantitatively with the experimental data, including particle size distribution [38]. Therefore, using a combination of mentioned software packages for simulation of the precipitation gives a better and more comprehensive understanding of the precipitation.

4.4 Parameter selection for simulation

In the present work, the thermodynamic and kinetic data required for the simulation work are taken from [89-91]: the TCFE7 and MOBFE2 databases were used for Papers I and II [37, 38], while TCFE8 and MOBFE3 databases were used for Papers IV and V [51, 52].

Since the input parameters, such as the interfacial energy, dislocation density and grain size, have a strong influence on the simulation results, these parameters deserve special

attention in modelling in e.g., TC-PRISMA, see Fig. 4.2. The interfacial energy, γ, has a cubic relationship with the nucleation and growth rates of precipitates, and is always calculated using physical models since it is difficult to measure directly [49]. To evaluate the interfacial energy, an extension of Becker's model has been implemented in TC-PRISMA, and the calculated value can be used in the modelling as a starting value for the interfacial energy. When setting up a simulation in TC-PRISMA a few candidate carbides are chosen, and the carbides formed during tempering are determined automatically.

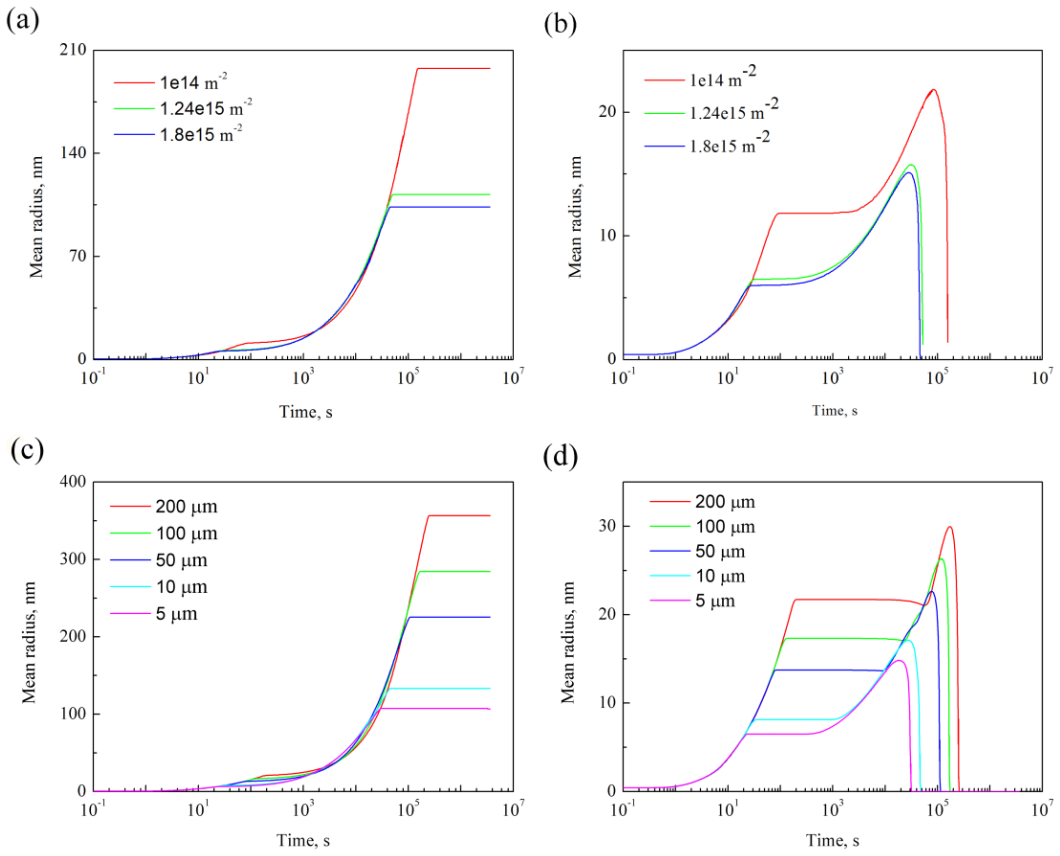

Fig. 4.2 Mean radii of M_7C_3 (a) and (b) of the alloy Fe-0.15C-4.0Cr tempered for different times, obtained from TC-PRISMA (solid lines) and experiments (symbols). Images are from [51].

The setting for the nucleation site type of precipitates could be obtained from the experimental observation, for example, the high density of dislocations is assumed to be the primary heterogeneous nucleation sites in martensite during tempering. Depending on the alloy system, the other nucleation site types e.g., bulk, grain boundaries and grain

corners, could also be used as nucleation sites. The supersaturated martensite is treated as a BCC structure in all the simulations.

The growth and coarsening of M_3C was simulated using DICTRA with a single cell system, composed of a martensitic matrix (BCC) and a M_3C nucleus. Different assumptions at the moving interface are employed to simulate the growth stage of M_3C under different interface conditions [20]. In the present work, only the elements Fe, Cr and C were considered to ensure the calculation could be handled in a reasonable time.

For the growth stage, the radius of the cell can be calculated from the relationship between the volume fraction of M_3C and the matrix cell size. Coarsening was simulated by setting the maximum size of the precipitate to 1.5 times the mean radius of all precipitates, according to the classical theory by Lifshitz, Slyozov and Wagner [80]. The composition of the nucleus was set e.g., to the same Cr/Fe ratio as for the matrix phase, depending on which type of growth mechanism was used. The matrix composition was equal to that of the substrate in accordance with the system and the start cell compositions. The increased pressure inside the precipitate due to its curved interface leads to an energy addition to the chemical potentials of all elements i.e., the Gibbs-Thomson effect. The details of all settings can be found in Papers IV and V.

Chapter 5 Experimental Methodology

In the present chapter, the experimental methodology used in this thesis is presented for microstructural characterization and identification and quantification of precipitates in the investigated Fe-C-Cr steels. Fig. 5.1 presents a schematic overview of the experimental procedures.

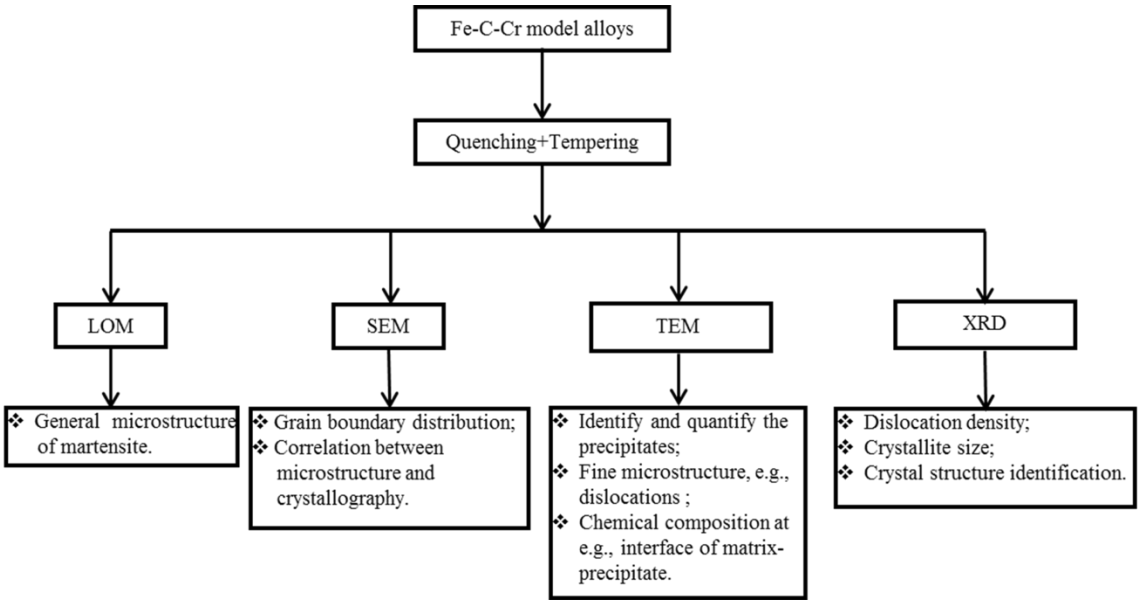

Fig. 5.1 Schematic of the experimental procedures followed in this thesis.

Chapter 5 Methodology

5.1 Material preparation

Since the Fe-C-Cr system forms the basic system for tool steels, four Fe-C-Cr steels with varying carbon and chromium contents were chosen as model alloys to investigate. In **Table 5.1**, the chemical compositions of the alloys studied in the present work are listed.

Table 5.1 Chemical compositions of the investigated alloys (in mass%).

Alloy	C	Cr	Si	Mn	S	Al	Fe
Fe-0.15C-1.0Cr	0.14	0.98	0.02	0.07	0.06	0.01	Bal.
Fe-0.15C-4.0Cr	0.16	4.05	0.02	0.08	0.05	0.02	Bal.
Fe-1C-1Cr	0.95	1.06	0.02	0.07	0.09	0.03	Bal.
Fe-1C-4Cr	0.88	4.12	0.03	0.08	0.05	0.02	Bal.

Samples (10×10×1 mm) were prepared from the hot-rolled plate, which is thin enough to enable a sufficient cooling rate throughout the sample upon quenching. All the samples were austenitized at 1100 ℃ for 10 min in a calibrated Entech tube furnace, followed by quenching in brine to room temperature. Then, the as-quenched samples were tempered for up to 5000 h at different temperatures from 500 ℃ to 700 ℃. Two different methods were employed to eliminate the influence of heating time, oxidation and decarburization during the tempering. The details of the heat treatments are listed in Table 5.2.

Table 5.2 Experimental conditions and equipment used for heat treatment in the present study.

Tempering time	5 s, 5min, 30 min	5 h, 100 h, 1000 h, 5000 h
Methods	Sn-Bi metal bath	Vacuum-sealed quartz tube in Muffle furnace

5.2 Light optical microscopy

Light optical microscopy (LOM) has been widely used in material science research. In LOM, visible light acts as the source and a system of lenses work as a magnifier to

enlarge the images of small features [24]. Even though the resolution and depth-of-field are limited by the wavelength of visible light (around 500 nm) [24], LOM can often give an overview of the martensitic microstructure, see Fig. 2.5.

5.3 Scanning electron microscopy

Scanning electron microscopy (SEM) is an instrument frequently used to investigate a wide range of materials. Compared with LOM, SEM has advantages in spatial resolution and depth-of-field. The SEM with a field emission gun (FEG) can achieve a resolution better than 1 nm. Thus, SEM can be used to reveal very fine microstructural features in materials. In FEG SEM, a coherent electron beam is generated from the field emission source, then the beam will interact with atoms in the sample, emitting different types of signals. Fig. 5.2 shows the different types of signals originating from different interaction depths. Signals such as secondary electrons and backscattered electrons emitted from the surface of sample are acquired by specialized detectors and transformed into corresponding images based on the position of the beam in the scan area [24].

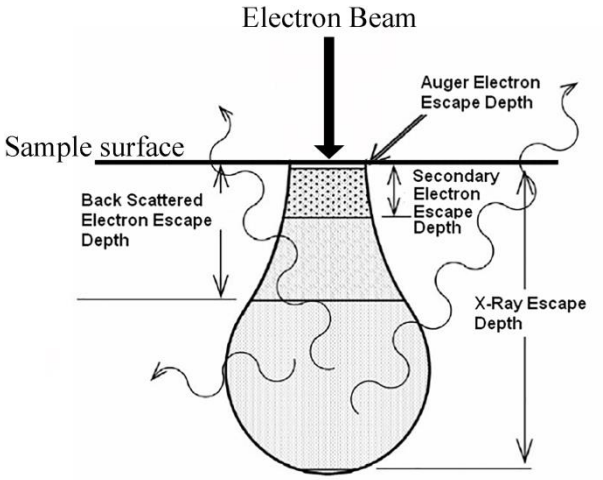

Fig.5.2 Schematic illustration of the signals from different interaction depths [24].

Electron micrographs are created by scanning the region of interest (ROI) in the sample with the electron beam and collecting the secondary electrons or backscattered electrons. The secondary electrons are emitted from outer shell electrons due to inelastic interactions between the primary electron beam and the sample. The secondary electrons

are generated from the surface or near-surface regions (5 to 50 nm depth) of the sample [24]. Thus, they give information about the topography of the sample surface scanned.

On the other hand, the backscattered electrons are generated from the quasi-elastic interaction of the incident electrons beam with the nucleus of atoms in the sample. After being backscattered or reflected from the sample, the trajectory of the incoming beam electrons changes significantly. The production of backscattered electrons is proportional to its atomic number: the larger the atomic number, the larger the amount of backscattered electrons. Thus, the backscattered electron image is composition sensitive (image contrast). Furthermore, the contrast also depends on the crystal orientation, the BSE yield will be different for different crystal orientations due to the electron channelling effect. This is the basis of the electron channelling contrast imaging (ECCI) technique [93]. In our study, ECCI was applied to reveal crystal defects such as lath boundaries and for quantifying the width of laths in a large volume (see Fig. 5.3).

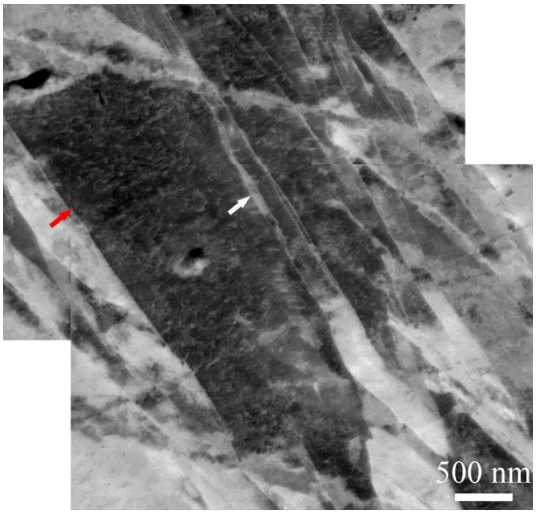

Fig. 5.3 ECCI of typical microstructure in Fe-0.15C-4.0Cr alloy after austenitizing at 1100 ℃ for 10 min, followed by quenching in brine to room temperature.

5.4 Electron backscatter diffraction

Electron backscatter diffraction (EBSD) in SEM is an accessory system widely used by material scientists for obtaining information on the crystallographic orientation of each

pixel in the scanned region of interest [24, 93]. In addition, this can provide other valuable quantitative microstructural information such as grain size, phase fraction and pixel-to-pixel misorientation. In a typical EBSD measurement set-up, the sample is tilted to 70^{o} from the horizontal position, which helps in obtaining sufficient backscattered electrons on the detector. Fig. 5.4 gives the typical settings and process of EBSD measurements. When the electron beam scans the tilted sample, some electrons may inelasticlly exit near to the Bragg angle and elastically diffract to form Kikuchi bands to produce diffraction pattern characteristic of the diffracting planes. These patterns are collected by an EBSD camera.

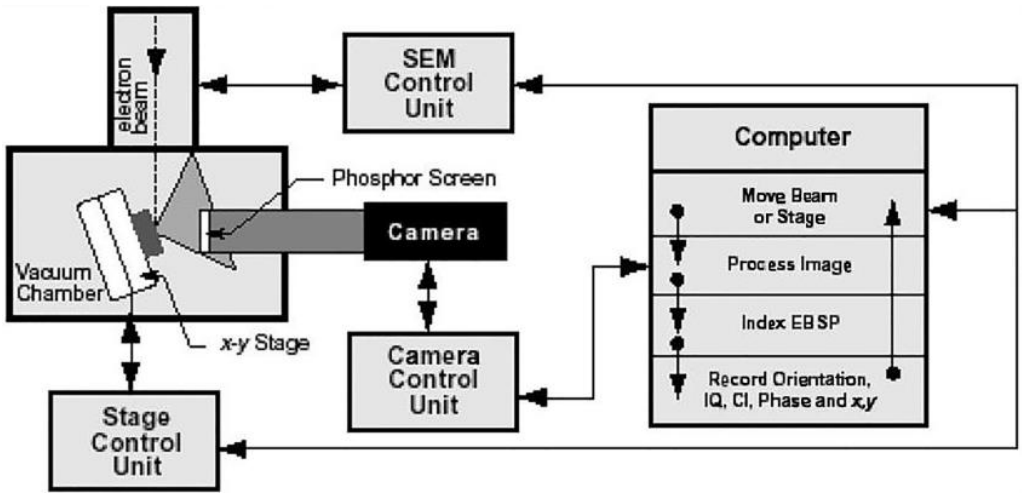

Fig. 5.4 Illustration of setting up for EBSD measurement, Image is from [93].

The orientation information of individual pixels in the scanned area is analyzed based on the reference diffraction patterns simulated for the specific crystallographic phases. Artifacts originating from the sample preparation could affect the results and thus the analysis of EBSD patterns. Therefore, utmost care is necessary at all levels for successful EBSD analysis. The term “misorientation” represents the orientation difference between the pixels compared to a reference system, which is helpful in identifying grains and other features such as laths, blocks and packets in martensite. Thus, the size of units such as sub-/ block, packet, can be evaluated by assigning limiting misorientation angles to these specific boundaries. In addition, the misorientation angle distribution, which represents the orientation angle between any two adjacent pixels in the scanned area, can

also be obtained to understand how different units such as laths, blocks and packets evolve.

The coupling of EBSD with BSE images provides an efficient approach for obtaining both a high-resolution image and crystallography for the microstructure. This technique has been successfully applied to the characterization of e.g., stacking faults, nanotwins and microbands [93]. In the present study, the interaction between the precipitates and migration of boundaries has been well characterized and described by this method, see Fig. 5.5.

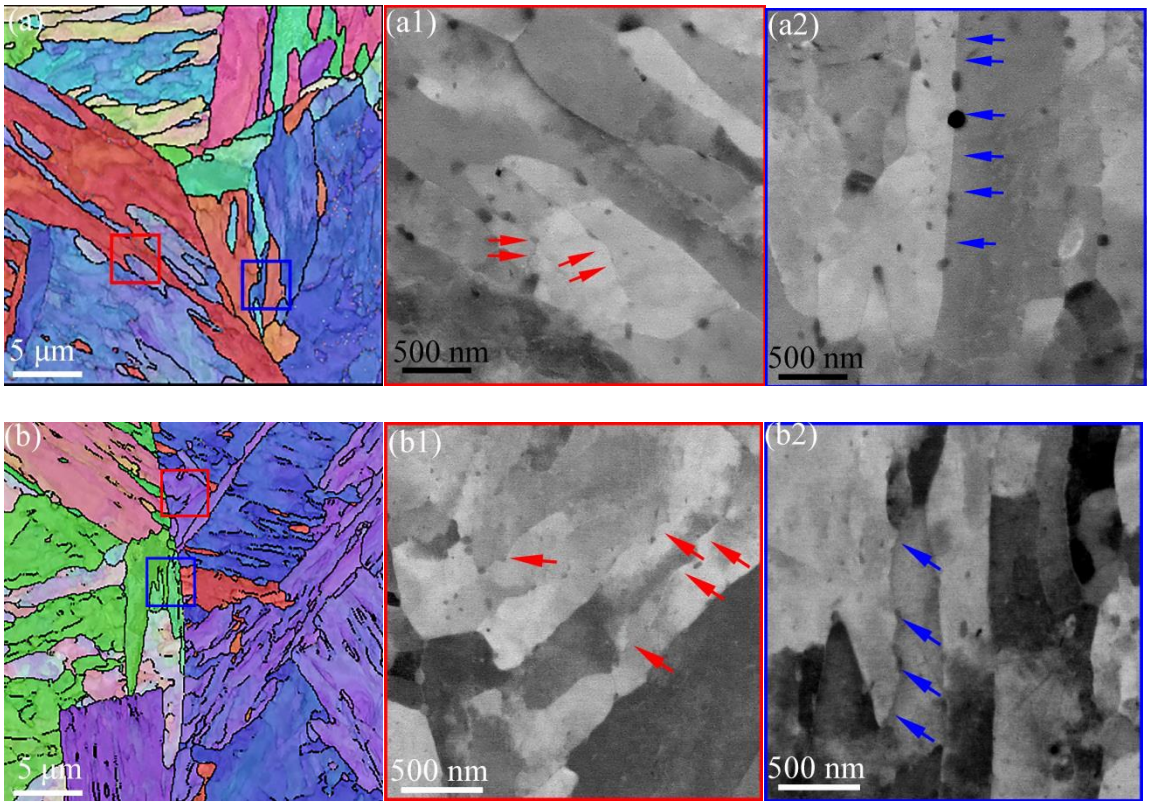

Fig. 5.5 Correlated EBSD-BSE images in (a), (a1) and (a2) for Fe-0.15C-4.0Cr alloy, and in (b), (b1) and (b2) for Fe-0.15C-1.0Cr alloy after being tempered for 30 min at 700 ℃. Black lines in IPF maps (a) and (b) show the boundaries with misorientation > 5 °. (a1, b1) and (a2, b2) are the areas marked in (a) and (b), respectively. Images are from [58].

5.5 Transmission electron microscope

Transmission electron microscopy (TEM) is based on the interaction between an energetic electron beam and an electron-transparent thin sample [24, 94]. Since the interaction volume between the transmitted electron beam and the sample is small, TEM provides a much higher spatial resolution than SEM. In particular, TEM is capable of imaging nano-sized structures such as dislocations and twins as well as conducting spectroscopy for composition analysis. Identifying the crystal structures and lattice parameters of various phases, crystallographic orientation relationships between adjacent grains or phases can also be performed using TEM diffraction.

Two types of TEM samples, i.e., thin foil and carbon extraction replica, have been commonly used in steels to study the different microstructural features. Compared to the thin foil TEM samples, the carbon extraction replicas have several advantages in the characterization of fine precipitates in steels: (1) a distinct contrast between the precipitates and the background makes semi-automatic (even automatic) measurements of the size distribution possible; (2) elimination of all possible influences of the matrix phase during chemical composition analysis; (3) large thin area available for TEM examination and statistical analysis; (4) avoiding a magnetic specimen that interacts with the electron beam. Hence, the carbon extraction replicas were preferred for quantitative analysis of the precipitates.

Information about the matrix phase and the relationship between the matrix and precipitate are lacking in the carbon extraction replica. For example, distribution of alloying elements at the interphase interfaces provides a proof of elemental diffusion during phase transformation. However, this type of information can help in understanding the precipitation reaction e.g., how the interface migrates at the early stage. Another important point to note is that some types of fine precipitate with low alloying elements might be lost during the carbon extraction replica preparation due to relatively faster dissolution compared to precipitates with high alloy content. Thus, thin foil TEM samples are also important for the precipitation study.

Selected area diffraction patterns (SADP) of the precipitate, in combination with its chemical composition analyzed by Energy-dispersive X-ray spectroscopy (EDXS), were used to identify the precipitates [95, 96]. Several similarly shaped particles were analyzed for each type of precipitate to ensure that the identification was correct. After the identification of the precipitates the particle size distribution (PSD) analysis was also performed using multiple TEM bright field images taken from the carbon replicas on copper grids. Automatic particle analysis was performed using the software Image J, and a considerable number (e.g., ~300) of precipitates were counted for each type of precipitate [52].

The projected area of the particles was converted to radii (assuming a spherical shape). The mean radius r_m of the precipitate j can be expressed by the total area A_j and number of particles counted (n):

$$r_m = \sqrt{\frac{1}{n}\sum_{j=1}^{n} A_j \Big/ \pi} \tag{5.1}$$

Based on the number of particles in each class, the PSD of each type of precipitate can be obtained.

Thin foil TEM samples can be prepared by either dual-jet electro-polishing or dual beam focused ion beam (FIB) instrument. The TEM foils often exhibit thickness variations close to the precipitates, since the matrix-precipitate interface is chemically weak and the precipitates are normally resistant to chemical polishing. This difference is clearly seen at regions close to large precipitates greater than 100 nm. For a quantitative and comparative analysis of composition across different phases such as in line-scans, the thickness of region of interest in the TEM foil should be uniform and thus allow application of an EDXS absorption correction using the Cliff-Lorimer thin-film approach [97, 98]. Therefore, FIB was employed in the present study to prepare the TEM thin foil samples to study the composition at matrix-carbide interface, see Fig. 5.6. The sample thickness of the region of interest was analyzed by the electron energy loss spectroscopy (EELS) based on absolute thickness measurements using the log-ratio method and was confirmed to have variations within 10% in thickness.

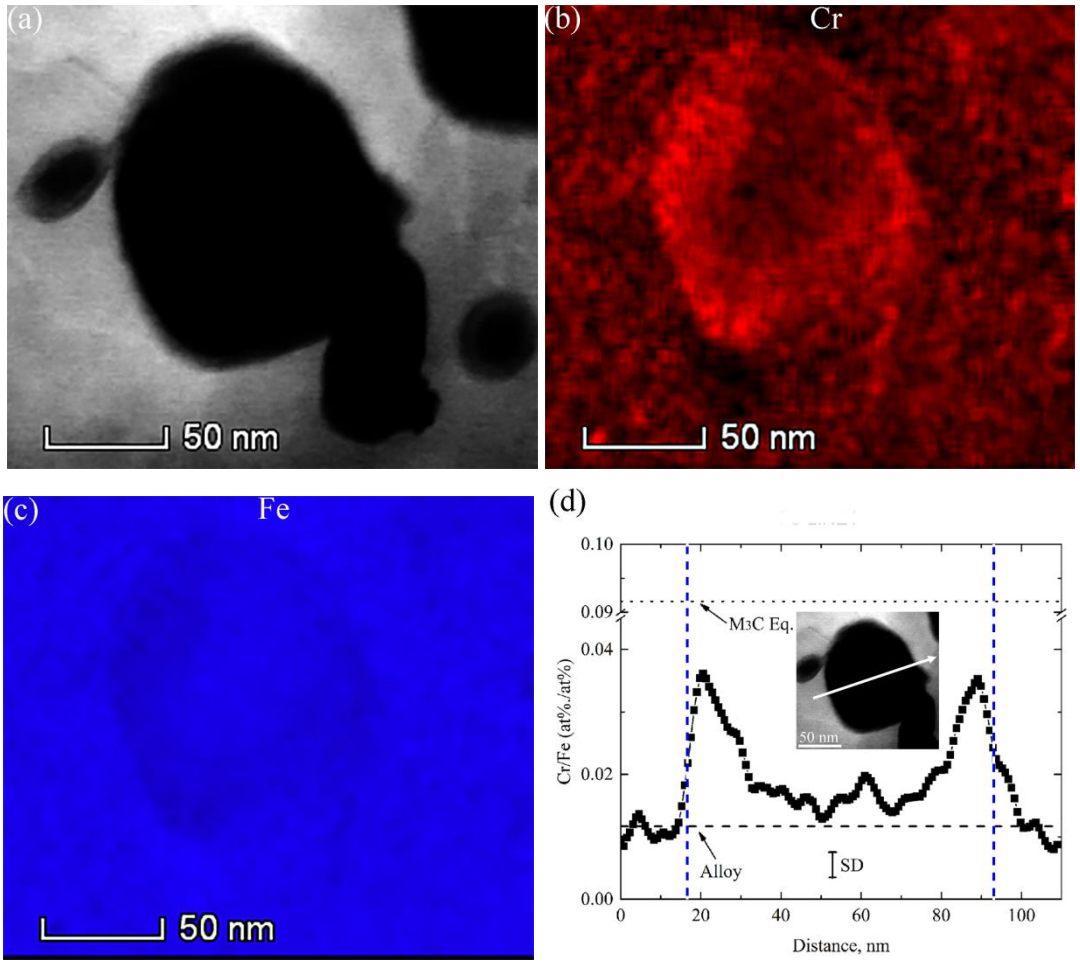

Fig. 5.6 TEM-EDS results for a thin foil sample cut by FIB from a Fe-1C-1Cr alloy after tempering at 500 ℃ for 30 min. (a) Bright field TEM image; TEM-EDS map of elemental Cr (b) and Fe (c); Analysis of line scan profiles across the interface of the precipitate and matrix.

5.6 X-ray diffraction

The crystal structure of a material can be analyzed using X-ray diffraction. The X-ray diffraction is based on the interaction of incident X-rays and the irradiated sample. X-rays are generated by a sealed tube source and then are directed towards the sample. X-rays are scattered by the atoms in the sample. Since a crystal has periodic array of atoms, diffraction occurs from the scattered radiation. A constructive interference occurs when some of the scattered rays satisfy Bragg's Law [24]:

$$n\lambda = 2d\sin\theta \tag{5.2}$$

Thus, the Bragg's law relates the wavelength (λ) of electromagnetic radiation to the diffraction angle (θ) and the lattice spacing (d) in a crystal.

The lattice spacing between the crystal planes in a cubic crystal with a lattice parameter *a* is given by [24]:

$$d_{hkl} = \frac{\alpha}{\sqrt{h^2 + k^2 + l^2}} \tag{5.3}$$

where *h, k, l* are the Miller indices of the crystal plane.

When a single crystallite is irradiated by a monochromatic X-ray, constructive interference occurs at several defined diffraction angles, which is shown by the diffraction peaks against 2 θ in XRD patterns.

If the crystal is strained, e.g., by an interstitial atom in BCC-ferrite, then the *d* space will be affected. According to Bragg's law the position of the peak corresponding to the specific planes that are affected will shift. This provides an approach to evaluate the solid solution interstitial atom in an as-quenched martensite based on the assumption that the peak shift is only caused by the pre-expected elements [56-58]. The peak broadening, as shown in Fig.5.7, can be analyzed to evaluate the crystallite size and dislocation density [73].

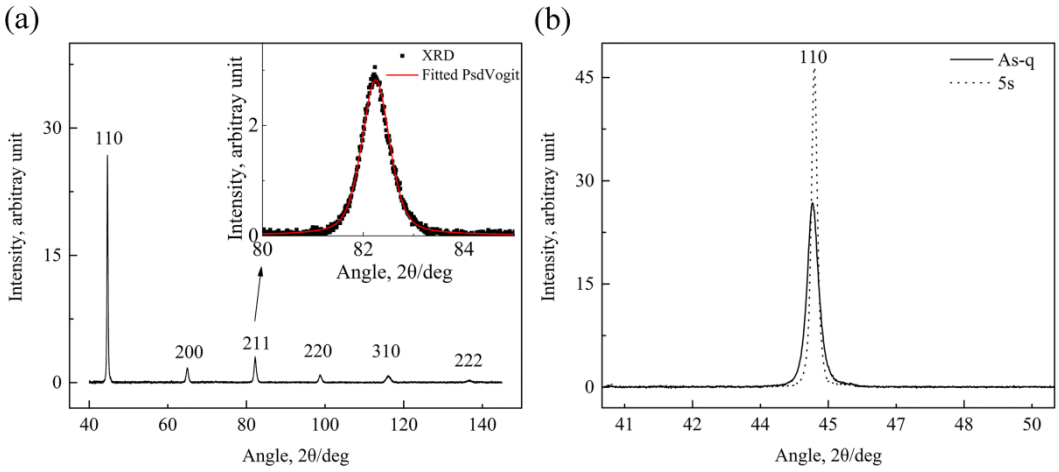

Fig. 5.7 (a) X-ray diffraction pattern of as-quenched Fe-0.15C-4.0Cr alloy, in which the 211 peak was fitted using a pseudo-Voigt function (insert image); (b) X-ray diffraction peak 110 for the Fe-0.15C-4.0Cr alloy in as-quenched and 5s at 700 ℃ tempered condition. Image are from [58].

5.7 Electrolytic extraction

The volume fraction together with mean radius of the precipitates will determine the effect of these precipitates on the bulk properties of the material, as mentioned earlier. Thus, quantitative analysis of the volume fraction of precipitates needs to be conducted. Electrolytic extraction (EE) is a method used to collect the residual phase (e.g., precipitates, inclusions) after the bulk of the sample has been dissolved in the electrolyte, which is based on the different dissolution resistance of phases in electrolyte [99], see Fig. 5.8.

The resistance towards the electrolyte depends on the alloys system and the studied object. A proper electrolyte is selected with a criterion that allows the matrix phase to dissolve as much as possible while the precipitates will be retained as much as possible. Since foreign contaminants can be introduced easily during the EE operation, careful cleaning of equipment and samples at each step is crucial for a successful EE experiment.

By utilizing techniques such as SEM, TEM and XRD, the particles collected from the electrolyte can be used to analysis the volume fraction, morphology and size of each type of precipitate [58, 95, 99].

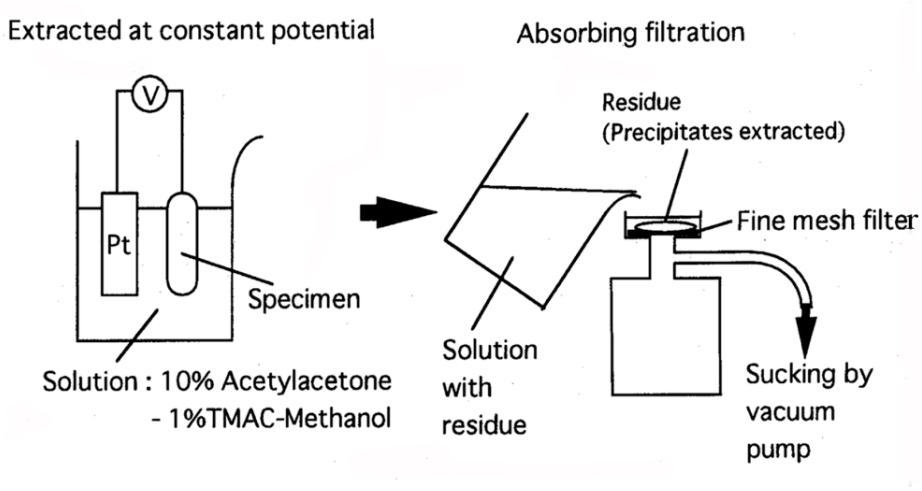

Fig. 5.8 Schematic of the Electrolytic Extraction (EE) process followed [99].

Chapter 6 Summary of appended papers

Paper I

Microstructure of martensite in Fe-C-Cr and its implications for modelling of carbide precipitation during tempering

In this work the microstructure of as-quenched martensite in the four model alloys (0.15C-1Cr, 0.15C-4Cr, 1C-1Cr, 1C-4Cr) was investigated using a combined set of microscopy tools. Thereafter, the microstructural parameters of martensite served as input for carbide precipitation modelling during tempering of martensite. The predicted modelling was conducted using Langer-Schwartz theory combined with the Kampmann-Wagner-Numerical (KWN) method, as implemented in the TC-PRISMA software. It was found that the lath martensite dominates the as-quenched microstructure in both low carbon steels. On the other hand, the as-quenched martensite in the high carbon steels is predominantly plate martensite with planar defects. . The ratio of high-angle to low-angle grain boundaries was found to increase with increasing Cr, which indicates that Cr has a similar effect on lath martensite microstructure as C. The parameters input such as dislocation density and grain size have a drastic effect on e.g., the mean size of precipitates.

Paper II

Quantitative modeling and experimental verification of carbide precipitation in a martensitic Fe-0.16 wt%C- 4.0 wt%Cr alloy

In this work, a martensitic Fe-0.16 wt.% C- 4.0 wt.% Cr alloy was tempered at 700 ℃ for up to 1000 h. Precipitation of carbides during tempering was investigated by experimental analysis and quantitative modelling. It was found that both M_7C_3 and $M_{23}C_6$ were formed at various grain boundaries and at dislocations inside individual laths of

martensite during tempering at 700 ℃. The prediction using Kampmann-Wagner modelling and TC-PRISMA software captures the main features of the carbide precipitation with M_7C_3 as the stable carbide and with a transient metastable phase of $M_{23}C_6$. The predicted size and volume fraction evolution are in good agreement with the experiments for the M_7C_3, but underestimates the size and overestimates the volume fraction of minority precipitate $M_{23}C_6$. It is concluded that with sound thermodynamic databank and physical parameter input, the simplified modelling scheme is a useful tool in the design and optimization of materials.

Paper III

Microstructure evolution during tempering of martensitic Fe-C-Cr alloys at 700 ℃

The microstructure evolution of two martensitic Fe-C-Cr alloys (Fe-0.15C-1/4 Cr) during tempering at 700 ℃ has been investigated. The microstructural parameters of martensite in both as-quenched and tempered conditions were quantitatively analyzed by using combined X-ray diffraction, transmission electron microscopy, electron channelling contrast imaging and electron backscatter diffraction. The findings shown that the high dislocation density of the as-quenched martensite decreased rapidly during the initial 5 seconds – tempering, but a further significant dislocation reduction was not observed after continued tempering for a long time. A clear difference in high-angle boundaries (HABs) was distinguished between the two alloys during tempering. The main reason for the different coarsening rates of HABs is the different pinning effect of carbide precipitates by the formed and coarsened carbides, i.e., fast coarsened M_3C in the low Cr steel and slow coarsened M_7C_3 in the high Cr steel during tempering.

Paper IV

Early stages of cementite precipitation during tempering of 1C-1Cr martensitic steel

In this work, the early stage of cementite (M_3C) precipitation from the as-quenched martensite during tempering at 500 and 700 ℃ was investigated in a Fe-1C-1Cr (mass %) alloy. At 500 ℃, no Cr enrichment was found through the M_3C/matrix interface and inside the M_3C after 5 minutes–tempering, while after further tempering to 30 minutes a clear enrichment of Cr at the shell surface region was observed. At 700 ℃, after

tempering for 5 seconds the core region of M_3C exhibited a Cr/Fe ratio equal to the bulk alloy concentration, and a shell surface region existed with a higher Cr concentration but which is still lower than the equilibrium value of M_3C. The experimental findings were further evaluated by modelling. It is clear that the diffusion simulation software DICTRA and precipitation simulation software TC-PRISMA captured neither the nucleation stage (TC-PRISMA) nor the growth phase (DICTRA and TC-PRISMA) during precipitation of M_3C. Based on these observations, the early stages of M_3C precipitation is discussed and further development of the precipitation modelling is suggested.

Paper V

Coarsening of cementite during tempering of a martensitic steel

In this study, the coarsening behavior of M_3C in a martensitic Fe-1C-1Cr (mass%) alloy during tempering at 700 ℃ was investigated by both experiments and kinetic precipitation modelling. The experiment results show that the large M_3C carbides are mostly located at grain boundaries. The size evolution of M_3C was agreed well with the experiments after the grain boundary diffusion effect was taken into the coarsening model. However, a log-normal distribution for the particle size distribution of M_3C was observed throughout the whole tempering process. This indicates that a classical steady-state coarsening theory is not fully adequate for practical purposes in the tempering of martensitic steels.

Chapter 7 Concluding remarks and future work

The efforts of the present thesis have been dedicated to increasing the knowledge of precipitation in martensitic Fe-C-Cr steels, which could aid the possibility of modelling the precipitation in martensitic steels. Martensitic steel is one of the most important types of steels and the precipitation evolution together with microstructure change during tempering is important to understand. In the present thesis, some important aspects of the precipitation have been discussed based on experiments and precipitation kinetic modelling. Through the systematic investigation on the precipitation of martensitic Fe-C-Cr steels, several conclusions can be drawn:

- In low carbon Fe-C-Cr alloys, the as-quenched martensitic microstructure becomes finer with increasing Cr content from 1.0 to 4.0 mass %. The ratio of high-angle to low-angle grain boundaries is found to increase with increasing Cr, which indicates that Cr has a similar effect on lath martensite microstructure as C. However, Cr addition only shows a negligible influence on the micro-hardness.
- During tempering at 700 ℃, faceted M_7C_3 and elongated $M_{23}C_6$ are nucleated at various boundaries and within the lath of maternsite in the Fe-0.15C-4.0Cr alloy. The adopted model taking the static tie-line across the bulk composition underestimates significantly the mean size of predominant carbides M_7C_3. The formed M_7C_3 grow under the NPLE condition and this is the reason for the deviation of the predicted result for carbide M_7C_3 compared to experiments from carbon extraction replicas at the initial beginning stage of precipitation.
- In two Fe-0.15 C-(1.0, 4.0) Cr alloys, high dislocation density of the as-quenched martensite reduces rapidly during the initial 5 seconds tempering at 700 ℃, but a further significant reduction in the dislocation density of tempered martensite was not found during the following few minutes of tempering. The martensitic

microstructures containing both coarse and fine lath coarsen slowly. While, a clear distinction between these two alloys was found regarding the mobility of units (high-angle) boundaries. The precipitate coarsening with a high/low rate pose little/effective hindrance for coarsening of the units, and thus this is the main reason for the microstructural difference during tempering.

- In a Fe-1.0C-1.0Cr (mass%) alloy, Cr enrichment at the interface zone between M_3C and the matrix occurred, while the Cr/Fe ratio inside M_3C is equal to the bulk Cr/Fe ratio after tempering at 700 ℃ for 5 seconds. After tempering at 500 ℃, an apparent enrichment of the Cr at M_3C/matrix interface was first observed after 30 minutes. Neither nucleation nor growth of M_3C can be captured very well by the simulation programmes (TC-PRISMA and DICTRA) used, and it is suggested that the nucleation model in TC-PRISMA is modified with respect to the allowed nucleus composition.

- In the long-tempered Fe-1.0C-1.0Cr (mass%) alloy, M_3C precipitates are located at the boundaries during the coarsening stage. The predicted size evolution of M_3C shows a good agreement with the experiments after grain boundary enhanced diffusion is taken into the coarsening model. The particle size distribution of M_3C, which maintains a log-normal distribution during the whole coarsening process, is discussed in terms of the prediction with the classical steady-state coarsening theory.

In order to fully understand and model the precipitation behavior in martensitic Fe-C-Cr alloys during tempering, a number of future challenges should be addressed:

- In the present work, the as-quenched microstructure has shown an effective influence on the precipitation during tempering. Since the martensitic microstructure is both chemical composition and process dependent, the microstructure of martensite formed under different conditions, e.g., varying cooling medium, may also vary considerably and thus affect the precipitation during the following tempering. However, the present work only considers the effect of chemical composition on the microstructure. Hence, a symmetric study on the as-quenched martensite formed at different conditions is important to understand the effect of microstructure on the

precipitation in a specific alloy during tempering. This information could help to model the precipitation in commercial martensitic steels.

- In the present work, a discrepancy has been found between the experimental and predicted results for the precipitation of the M_7C_3 in Fe-0.15C-4.0Cr (mass%) alloy at the early stage. The primary proposed explanation is that the growth of precipitates is under a NPLE mechanism, in which the fast diffusion of carbon controls the interface movement. However, solid evidence for this, which could be the distribution of chemical composition at the interface of precipitates-matrix phase and within the precipitate, is still lacking. Thus, an analysis of short-term tempered samples by advanced experimental methods e.g., Atom-probe tomography (APT) and HRTEM, could shed some light on the governing condition at the carbide/matrix phase interface: PE, NPLE, PLE or something else.
- In the present work, the effect of grain boundary diffusion on coarsening of precipitation has been quantitatively studied for the first time in a martensitic Fe–1.0C–1.0Cr (mass%) alloy during tempering. To gain an even better quantitative understanding of the contribution of grain boundaries on the precipitation, the precipitation in the martensitic steels with varying grain size should be pursed. This could help to improve the coarsening modelling and design of materials with specific grain size or types of grain boundaries to tailor the mechanical properties of martensitic steels.
- In the present thesis, the microstructural evolution of two low carbon steels during tempering has been well characterized. However, the mechanical properties for both steels are lacking. Thus, the mechanical properties should be further investigated by e.g., nano-indentation and tensile tests. This could hint e.g., how the changing microstructure of martensitic steels during tempering is related to its mechanical properties, and which factors would contribute to the hardness or strength.
- In the present work, the characterization of the as-quenched and tempered martensitic microstructure, which served as input parameters for the modelling, is based on 2-D sections by TEM, EBSD or SEM. However, the hierarchical martensite may not be represented very well by the 2-D sections parameters due to a sectioning effect, which could influence the modelling results directly. Thus, a more scientific approach needs

to be developed to reveal the full features of martensite, for instance, 3-D re-constructed maps by EBSD. This could provide a way to present the plate- and lath-shaped martensite, and thus to improve the modelling results.

Acknowledgements

First of all, I would like to express my sincere gratitude to my principle supervisor Joakim Odqvist. Thanks for his continuous guidance and encouragement during this study. I cannot image how the past time will be without his invaluable support and inspiration. I would also give my great gratitude to my co-supervisor Peter Hedström. Thanks for his enthusiasm and effort put into this work. Both of them evoke me to think deeper and broader in all long discussions, which definitely helped to improve and enhance my work a lot. I will remember all of their efforts put on me during this journey.

I would like to give my heartfelt gratitude to Prasath Babu. Thanks for his support and valuable discussions on the experiments and data analysis, it has been a precious experience for me to work with him. I sincerely appreciate his unselfish help.

I would like to acknowledge Annika Borgenstam for inviteting me to participate in a new project, leading tolots of fun and fruitful discussions, and supporting the last period of my PhD journey.

I really appreciate the helpful guidance to the TC-PRISMA software and valuable discussions from Dr. Qing Chen at Thermo-Calc Software AB. Fredrik Lindberg and Niklas Pettersson at Swerea KIMAB are thanked for their guidance to the preparation of carbon replica samples and for help with the TEM. Rafeal Borrajo-Peleaz is thanked for help with the TEM. A special thanks goes to Henrik Jesperson (formerly with Uddeholms AB) and Maria Kvarnström at Uddeholms AB for their support with some of the TEM work. Andrey Karasev and Hongying Du at KTH are thanked for their introduction and guidance to the electrolytic extraction. I wish express my gratitude to Wenli Long at KTH, for her support on my lab work and also on my life, I will not forget the mooncake, steamed stuffed bun etc. she shared.

Acknowledgements

I also would like to give my honest gratitude to my friends for their company, thanks to them my life in Sweden has been far from dull and boring. I will never forget the funny time together with them during “fika”, jog, travel and party. Because of them, I always have a feeling like home: my sisters and brothers around me. Here, I will not write down any names since I know they know who they are!

This work was performed within the VINN Excellence Center Hero-m, financed by VINNOVA, the Swedish Governmental Agency for Innovation Systems, Swedish industry and KTH Royal Institute of Technology. Support from the EU EIT KIC Raw Materials project, Stiftelsen Axel Hultgren Fond, The Foundation for Applied Thermodynamics (STT), travel grants from Olle Erikssons Stiftelse för materialteknik, Bergshögskolans Jubileumsfond, and a research grant from the Swedish Steel Producers’ Association are gratefully acknowledged.

Finally, I would like to express my greatest gratitude to my parents and my wife (海炜) for their endless support. I would not have arrived here without their understanding and support, especially in the past one year after my daughter was born. Really, I’m also grateful to my daughter Molly (乐心), and the joy I got from her.

Bibliography

[1] H.K.D.H. Bhadeshia, R. Honeycombe, Steels: microstructure and properties. The tempering of martensite steels (Oxford, OX: United Kingdom Elsevier Publishing Company, 2006), 183-208.

[2] G. Krauss, Martensite in steel: strength and structure. Mater Sci Eng A, 1999, 273-275: 40-57.

[3] G. Krauss, Tempering of lath martensite in low and medium carbon steels: assessment and challenges. Steel Res Int, 2017, 88(10): 1700038. doi:10.1002/srin.201700038.

[4] G.E. Totten, Steel heat treatment: Metallurgy and technologies (London, LON: LLC Taylor & Francis Group, 2006), p207.

[5] C.S Smith, A history of martensite: Early ideas on the structure of steel, in: G.B. Olson, W.S. Owen (Eds.), Martensite, ASM Int., Materials Park, OH, 1992, pp. 21-39.

[6] V. Velay, G. Bernhart, L. Penazzi, Cyclic behavior modelling of a tempered martensitic hot work tool steel, Int. J. Plasticity, 2006, 22 (3): 459-496.

[7] A. Medvedeva, J.Bergström, S.Gunnarsson, J. Andersson, High-temperature properties and microstructural stability of hot-work tool steels. Mater Sci Eng A, 2009, 523(1-2): 39-46.

[8] S. M. H. Hoseiny, Influence of microstructure on the machinability of prehardened mould steels. Ph.D thesis, Chalmers University of Technology. 2011.

[9] F. Abe, M. Taneike, K. Sawada, Alloy design of creep resistant 9Cr steel using a dispersion of nano-sized carbonitrides. Int J Pres Ves Pip, 2007, 84 (1-2): 3-12.

[10] M.C. Mataya, R.A. Fournelle, Fatigue behavior of a nial precipitation hardening medium carbon steel. Metall Trans A, 1978, 9 (7): 917-925.

[11] M.F. Ashby, H. Shercliff, D. Cebon, Materials: Engineering, Science, Processing and Design, Published by Elsevier, L td. Butterworth-Heinemann. 2007, 209.

[12] J.W. Martin, Precipitation hardening. Butterworth-Heinemann, Oxford. 1968.

[13] S. Yamasaki, Modelling precipitation of carbides in martensitic Steels. Ph.D thesis, Darwin College, University of Cambridge. 2004.

[14] P. Michaud, D. Deslagnes, P. Lamesle, M. H. Mathon, C. Levaillant, The effect of the addition of alloying elements on carbide precipitation and mechanical properties in 5% chromium martensitic steels. Acta Mater, 2007, 55 (14): 4877-4889.

[15] T. Ohmura, K. Tsuzaki, S. Matsuoka, Evaluation of the matrix strength of Fe-0.4 wt% C tempered martensite using nanoindentation techniques. Philos Mag A, 2002, 82(10): 1903-1910.

[16] T. Ohmura, T. Hara, K. Tsuzaki, Evaluation of temper softening behavior of Fe-C binary martensitic steels by nanoindentation. Scr Mater, 2003, 49(12):1157-1162.

[17] T. Ohmura, T. Hara, K. Tsuzaki, Relationship between nanohardness and microstructures in high-purity Fe-C as-quenched and quench-tempered martensite. J Mater Res, 2003, 18(6):1465-1470.

[18] T. Ohmura, K. Tsuzaki, Evaluation of matrix strength of Fe-C as-quenched and quench-tempered martensite using nanoindentation techniques. J Phys IV France, 2003, 112: 267-270.

[19] T. Ohmura, T. Hara, K. Tsuzaki, H. Nakatsu, Y. Tamura, Mechanical characterization of secondary-hardening martensitic steel using nanoindentation. J Mater Res, 2004, 19(1): 79–84.

[20] C. E. I. C. Ohlund, E. Schlangen, S. Erik Offerman, The kinetics of softening and microstructure evolution of martensite in Fe-C-Mn steel during tempering at 300 ℃. Mater Sci Eng A, 2013, 560: 351–357.

[21] N. Mebarki, D. Delagnes, P. Lamesle, F. Delmas, C. Levaillant, Relationship between microstructure and mechanical properties of a 5% Cr tempered martensitic tool steel. Mater Sci Eng A, 2004, 387–389: 171–175

[22] M. A. Asadabad, S. Kheirandish, A. J. Novinrooz, Microstructural and mechanical behavior of 4.5Cr-2W-0.25V-0.1C steel. Mater Sci Eng A, 2010, 527 (6): 1612–1616.

[23] J. Allison, D. Backman, L. Christodoulou Integrated computational materials engineering: A new paradigm for the global materials profession. JOM, 2006, 58(11): 25-27.

[24] E. J. Mittemeijer, Fundamentals of materials science, the microstructure-property relationship using metals as model systems. Springer-Verlag Berlin Heidelberg, 2010.

[25] E. Kozeschnik, Modelling Solid-State Precipitation, (New York, NY: Momentum Press, LLC, 2013). p38, p76–93, p351.

[26] D.N. Seidman, Three-Dimensional atom-probe tomography: advances and applications. Annu Rev Mater Res, 2007, 37: 127–158.

[27] D.N. Seidman, K. Stiller, An atom-probe tomography primer. MRS Bull, 2009. 34: 717–724.

[28] H. Zurob, C. Hutchinson, Y. Bréchet, G. Purdy, recrystallization of microalloyed austenite: effect of coupling recovery, precipitation and recrystallization. Acta Mater, 2002, 50 (12): 3077–3094.

[29] T. Gladman, The physical metallurgy of microalloyed steels. The institute of materials, London, 2002.

[30] M. Hillert, Inhibition of grain-growth by 2nd-phase particles. Acta Metall, 1988, 36(12): 3177–3181.

[31] F. Abe, Bainitic and martensitic creep-resistant steels. Curr Opin Solid State Mater Sci, 2004, 8: 305–311.

[32] T. Tschiyama, Y. Miyamoto, S. Takaki, Recrystallization of lath martensite with bulge nucleation and growth mechanism. ISIJ Int, 2001, 41(9): 1047–1052.

[33] A. Borgenstam, A. Engström, L. Höglund, J. Ågren, A tool for simulation of diffusional transformations in alloys. J Phase Equilib, 2000, 21: 269–280.

[34] K. Frisk, Simulation of precipitation of secondary carbides in hot work tool steels. Mater Sci Tech, 2012, 28 (3): 288–294.

[35] H. J. Jou, P. Voorhees, G. B. Olson, Computer simulations for the prediction of microstructure/property variation in aero turbine disks. Proc. Superalloys, Champion, PA, USA, September 2004, TMS, 877-886.

[36] L. Q. Cheng, C. M. Brakman, B. M. Korevaar, E. J. Mittemeijer, The tempering of iron-carbon martensite; dilatometric and calorimetric analysis. Metall Trans A. 1988, 19 (10): 2415–2426.

[37] Z. Y. Hou, P. Babu, P. Hedström, J. Odqvist, Early growth of cementite in tempered martensitic steel 1C1Cr. In manuscript.

[38] Z.Y. Hou, P. Babu, P. Hedström, J. Odqvist, A study of coarsening of cementite in an Fe-1C- 1Cr alloy. In manuscript.

[39] J. Janovec, M. Svoboda, A. Výrostková, A. Kroupa, Time-temperature-precipitation diagrams of carbide evolution in low alloy steels. Mater Sci Eng A, 2005, 402 (1–2): 288–293.

[40] K. Frisk, Simulation of precipitation of secondary carbides in hot work tool steels. Mater Sci Technol, 2012, 28 (3): 288–294.

[41] X. B. Hu, M. Zhang, X. C. Wu, L. Li, Simulations of coarsening behavior for $M_{23}C_6$ carbides in AISI H13 steel. J Mater Sci Technol, 2006, 22(2): 153–158.

[42] M. Perez, A. Deschamps, Microscopic modelling of simultaneous two phase precipitation: application to carbide precipitation in low carbon steels. Mater Sci Eng A, 2003, 360 (1–2): 214–219.

[43] P. F. Shi, A. Engström, B. Sundman, J. Ågren, Thermodynamic calculations and kinetic simulations of some advanced materials. Mater Sci Forum, 2011, 675–677: 961–974.

[44] A. Costa e Silva, L. Nakamura, F. Rizzo, Application of computational modeling to the kinetics of precipitation of aluminum nitride in steels. J Min Metall B, 2012, 48(3): 471–476.

[45] R. Mukherjee, T. A. Abinandanan, M. P. Gururajan, Phase field study of precipitate growth: Effect of misfit strain and interface curvature. Acta Mater, 2009, 57(13): 3947–3954.

[46] L. Q. Chen, Phase-field models for microstructure evolution. Annu Rev Mater Res, 2002, 32: 113–140.

[47] W. Cao, S. L. Chen, F. Zhang, K. Wu, Y. Yang, Y.A. Chang, R. Schmid-Fetzer, W. A. Oates, PANDAT software with PanEngine, PanOptimizer and PanPrecipitation for multi-component phase diagram calculation and materials property simulation. Calphad, 2009, 33(2): 328–342.

[48] N. Fujita, Modelling carbide precipitation in alloy steels. Ph.D thesis, University of Cambrige, 2000.

[49] Q. Chen, J. Jeppsson, J. Ågren, Analytical treatment of diffusion during precipitate growth in multicomponent systems. Acta Mater, 2008, 56(8): 1890–1896.

[50] O. Prat, J. García, D. Rojas, C. Carrasco, G. Inden, Investigations on the growth kinetics of laves phase precipitates in 12% Cr creep-resistant steels: experimental and DICTRA calculations. Acta Mater, 2010, 58(18): 6142–6153.

[51] Z.Y. Hou, P. Hedström, Y.B. Xu, D. Wu, J. Odqvist, Microstructure of martensite in Fe-C-Cr and its implications for modelling of carbide precipitation during tempering. ISIJ Int, 2014, 54(11): 2649–2656.

[52] Z.Y. Hou, P. Hedström, Q. Chen, Y.B. Xu, W. Di, J. Odqvist, Quantitative modeling and experimental verification of carbide precipitation in a martensitic Fe-0.16wt%C-4.0wt%Cr alloy. Calphad, 2016, 53:39–48.

[53] L. Delaey, Diffusionless transformations. In: Cahn R W, Haasen P, Kramer E J (eds.) Materials Science and Technology, Vol. 5, Phase Transformations in Materials. VCH, Weinheim, Germany, 1991.

[54] B.C. Muddle, J.F. Nie, Martensite, Encyclopedia of materials: science and technology, Elsevier Science Ltd. 2001, 5189–5193.

[55] B. Hutchinson, J. Hagström, O. Karlsson, D. Lindell, N. Tornberg, F. Lindberg, M. Thuvander, Microstructures and hardness of as-quenched martensites (0.1-0.5%C). Acta Mater, 2011, 59(14): 5845–5858.

[56] J. W. Christian, Tetragonal martensites in ferrous alloys-a critique. Materials transactions JIM, 1992, 33(3): 208–214.

[57] L. Cheng, A. Böttger, T. H. Keijser, Lattice parameters of iron-carbon and iron-nitrogen martensite and austenites. Scr Metal, 1990, 24: 509–514.

[58] Z. Y. Hou, P. Babu, P. Hedström, J. Odqvist, Microstructure evolution during tempering of martensitic Fe-C-Cr alloys at 700 °C, J Mater Sci, 2018, 53(9): 6939–6950.

[59] G. Kruss, A.R. Marder, The morphology of martensite in iron alloys. Metall Trans 1971, 2: 2343–2357.

[60] S. Morito, J. Niskawa, T. Maki, Dislocation density within lath martensite in Fe-C and Fe-Ni alloys. ISIJ Int, 2003, 43 (9): 1475–1477.

[61] S. Morito, H. Tanaka, R. Konishi, T. Furuhara, T. Maki, The morphology and crystallography of lath martensite in Fe-C alloys. Acta Mater, 2003, 51 (6): 1789–1799.

[62] T. Maki, Microstructure and mechanical behavior of ferrous martensite. Mater Sci Forum, 1990, 56-58: 157–168.

[63] M. Umemoto, K. Minoda, I. Tamura, Some characteristics of the substructure of lenticular martensite in Fe-Ni-C alloys, Metallography. 1982, 15(2): 177–191.

[64] M. Umemoto, E.Yoshitake, I. Tamura, The morphology of martensite in Fe-C, Fe-Ni-C and Fe-C-Cr alloys. J Mater Sci, 1983, 18(10): 2893–2904.

[65] P.M. Kelly, J. Nutting, The martensite transformation in carbon steels. Proc Roy Soc London A, 1960, 259: 45–48.

[66] P. M. Kelly, The martensite transformation in steels with low stacking fault energy. Acta Metall, 1965, 13(6): 635–646.

[67] L. Morsdorf, C.C. Tasan, D. Ponge, D. Raabe, 3D structural and atomic-scale analysis of lath martensite: effect of the transformation sequence. Acta Mater, 2015, 95: 366–377.

[68] B. B. He, M. X. Huang, Revealing the intrinsic nanohardness of lath martensite in low carbon steel. Metall Mater Trans A, 2015, 46 (2): 688–694.

[69] A. Stormvinter, P. Hedström, A. Borgenstam, Transmission electron microscopy study of plate martensite formation in high-carbon low alloy steels. J Mater Sci Technol, 2013, 29 (4): 373–379.

[70] T. Furuhara, S. Morito, T. Maki, Morphology, substructure and crystallography of lath martensite in Fe-C alloys. J Phys IV France, 2003, 112(1): 255–258.

[71] S. Morito, X. Huang, T. Furuhara, T. Maki, N. Hansen, The morphology and crystallography of lath martensite in alloy steels. Acta Mater, 2006, 54 (13): 5323–5331.

[72] S. Morito, Y. Adachi, T. Ohba, Morphology and crystallography of sub-blocks in ultra-low carbon lath martensite steel. Mater Trans, 2009, 50(8): 1919–1923.

[73] S. Takebayashi, T. Kuniedai, N. Yoshinaga, K. Ushioda, S. Ogata, Comparison of the dislocation density in martensitic steels evaluated by some X-ray diffraction methods. ISIJ Int, 2010, 50(6): 875–882.

[74] A. Stormvinter, P. Hedström, A. Borgenstam, Investigation of lath and plate martensite in a carbon steel. Solid State Phenomena, 2011, 172–174: 61–66.

[75] H.Y. Lee, H.W. Yen, H.T. Chang, J.R. Yang, Substructures of martensite in Fe–1C–17Cr stainless steel. Scr Mater, 2010, 62(9): 670–673

[76] A.T.W. Barrow, J.-H. Kang, P.E.J. Rivera-Díaz-del-Castillo, The ε→η→θ transition in 100Cr6 and its effect on mechanical properties. Acta Mater, 2012, 60: 2805–2815

[77] D. Kashchiev, Nucleation: basic theory with applications, Butterworth Heinemann, Oxford, 2000.

[78] R. Kammann, R. Wagner, Softening: kinetics of precipitation in metastable binary alloys-theory and application to Cu-1.9 at % Ti and Ni-14 at % Al. in decoposition of Alloys: the Early stages. P. Haasen,V. Gerold, R.Wagner and M.F. Ashby, eds., Pergamon Press, Oxford. 1984.

[79] M. Hillert, Paraequilibrium, Internal Report, Swedish Institute for Metal Research, Stockholm, 1953, appeared in Thermodynamics and Phase Transformations, The Selected Works of Mats Hillert, J. Ågren, Y. Bréchet, C. Hutchinson, J. Philibert, and G. Purdy, eds., EPD Science, Les Ulis, Cedex, France, 2006, pp. 9–24

[80] I. M. Lifshitz, V. V. Slyosov, The kinetics of precipitation from supersaturated solid solutions. J Phys Chem Solid, 1961, 19 (1–2): 35–50.

[81] R. A. Oriani, Ostwald ripening of precipitates in solid matrices. Acta Metall, 1964, 12: 1399–1409.

[82] J. D. Robson, Modelling the overlap of nucleation, growth and coarsening during precipitation. Acta Mater, 2004, 52: 4669–4676.

[83] D. H. Jack, K. H. Jack, Carbides and nitrides in steel. Mater Sci Eng, 1973, 11(1):1–27

[84] S. S. Babu, K. Hono, T. Sakurai, APFIM studies on martensite tempering of Fe–C–Si –Mn low alloy steel. Appl Surf Sci, 1993, 67(1–4): 321–327.

[85] C. Zhu, X. Y. Xiong, A. Cerezo, R. Hardwicke, G. Krauss, G. D. W. Smith, Three–

dimensional atom probe characterization of alloy element partitioning in cementite during tempering of alloy steel. Ultramicroscopy, 2007, 107(9): 808–812.

[86] A.J. Clarke, M.K. Miller, R.D. Field, D.R. Coughlin, P.J. Gibbs, K.D. Clarke, D.J. Alexander, K.A. Powers, P. A. Papin, G. Krauss, Atomic and nanoscale chemical and structural changes in quenched and tempered 4340 steel. Acta Mater, 2014, 77:17–27.

[87] W. Song, J. Appen, P. Choic, R. Dronskowski, D. Raabe, W. Bleck, Atomic-scale investigation of ε and θ precipitates in bainite in 100Cr6 bearing steel by atom probe tomography and ab initio calculations. Acta Mater, 2013, 61(20): 7582–7590.

[88] G. Stechauner, E. Kozeschnik, Assessment of substitutional self-diffusion along short-circuit, paths in Al, Fe and Ni. Calphad, 2014, 47: 92–99.

[89] Thermo-Calc Softerware TCFE 7 Steels/Fe/alloys database version 7, (accessed 30 August 2017).

[90] The Diffusion Module (DICTRA) User Guide 2017a (accessed 30 August 2017).

[91] The Precipitation Module (TC-PRISMA) User Guide 2017b (accessed 23 November 2017).

[92] J. O. Andersson, T. Helander, L. Höglund, P. F. Shi, B. Sundman, Thermo-Calc and DICTRA, computational tools for materials science. Calphad, 2002, 26: 273–312.

[93] I. Gutierrez-Urrutia, S. Zaefferer, D. Raabe, Toward the quantitative characterization of deformation structures in the SEM. JOM 2013, 65(9): 1229–1236.

[94] D. V. Sridhara Rao, K. Muraleedharan, C. J. Humphreys, TEM specimen preparation techniques. Microscopy: Science, Technology, Applications and Education A. Méndez-Vilas and J. Díaz (Eds.), 2010, 1232–1244.

[95] M. J. Donachie, O. H. Kriege, Phase extraction and analysis in super alloys-summary of investigation by ASTM committee E-4 task group 1. J Mater, 1972, 7: 269–278.

[96] K. L. Lin, Phase identification using series of selected area diffraction patterns and energy dispersive spectrometry within TEM, Microsc Res, 2014, 2: 57–66.

[97] Y. Q. Chen, R. Prasath babu, T. J. A. Slater, M. W. Bai, R. Mitchell, O. Ciuca, M. Preuss, S. J. Haigh, An investigation of diffusion-mediated cyclic coarsening and reversal coarsening in an advanced Ni-based superalloy. Acta Mater, 2016, 110: 295–305.

[98] M. Watanabe, D. Williams, The quantitative analysis of thin specimens: a review of progress from the Cliff-Lorimer to the new ζ-factor methods. J Microsc-Oxford, 2006, 221: 89–109.

[99] A. L. Rivas, E. Vidal, D. K. Matlock, J. G. Speer, Electrochemical extraction of microalloy carbides in Nb-steel. Revista de Metalurgia, 2008, 44(5): 447–456.